



HAL
open science

Finite plate elements with variable kinematics based on Sublaminated Generalized Unified Formulation

Girolamo Di Cara, Michele d'Ottavio, Thi Le, Olivier Polit

► To cite this version:

Girolamo Di Cara, Michele d'Ottavio, Thi Le, Olivier Polit. Finite plate elements with variable kinematics based on Sublaminated Generalized Unified Formulation. *Mechanics of Advanced Materials and Structures*, 2022, 30 (5), pp.1031-1049. 10.1080/15376494.2022.2126568 . hal-04153723

HAL Id: hal-04153723

<https://hal.science/hal-04153723>

Submitted on 6 Jul 2023

HAL is a multi-disciplinary open access archive for the deposit and dissemination of scientific research documents, whether they are published or not. The documents may come from teaching and research institutions in France or abroad, or from public or private research centers.

L'archive ouverte pluridisciplinaire **HAL**, est destinée au dépôt et à la diffusion de documents scientifiques de niveau recherche, publiés ou non, émanant des établissements d'enseignement et de recherche français ou étrangers, des laboratoires publics ou privés.

range of engineering applications [3, 4]. A discussion about sandwich panels’ applications with respect to their eco-efficiency in view of an environmental footprint reduction of structures has been recently provided by Resende Oliveira *et al.* [5]

The analysis and design of composite sandwich panels requires refined models to cope with the strong mismatch between facings and core in terms of mechanical stiffness and geometric thickness. In fact, the strong face-core heterogeneity renders classical models for composite structures, such as *Classical Lamination Theory* (CLT) or *First order Shear Deformation Theory* (FSDT), inappropriate for evaluating bending deflections or vibration characteristics [6]. The need for detailed models is even more stringent if the attention is to be given to local stress response, which is a necessary step for a reliable prediction of the complex failure modes that characterise sandwich panels [7, 8]. As pointed out by Birman and Kardomateas [9], refined models are mandatory also in view of resolving multifield interactions and/or cross-scaling effects, which constitute relevant axis of development towards advanced sandwich applications. For instance, in order to improve the fidelity of the macro/meso-scale models that are customarily employed for the sizing of built-up panel structures, homogenization schemes have been recently proposed that take into account the cellular structure of many employed core micro-structures [10–12].

A large number of refined, high-order two-dimensional (2D) models have been thus proposed with the aim of attaining sufficient accuracy without resorting to computationally expensive full three-dimensional (3D) models. Early developments have been exhaustively summarised and assessed by Noor and Burton [13, 14], for more recent overviews we refer to [15–19]. Over the last years, it is worth mentioning the extension from 1D (beams or wide plates) to 2D plate models of the Enhanced High-order Sandwich Panel Theory (EHSAPT) [20] and its extension towards geometrically nonlinear analysis [21].

Since they rely on *ad hoc* assumptions, the accuracy of such axiomatically derived structural models is problem-dependent, for it depends on the physics of the considered problem (materials, geometry, loading . . .) as well as on the output quantity of interest in the analysis. The variational-asymptotic approach is a mathematically very elegant manner to cope with this fundamental issue of reduced-order models [22], and it has conducted to relevant applications in the field of the mechanical response of sandwich structures [23, 24]. However, its generalization to complex problems, e.g., involving multifield couplings, still requires a heavy mathematical effort.

A very flexible and general framework for implementing virtually any kind of structural 1D beam and 2D plate/shell models has been proposed by Carrera with his Unified Formulation (CUF) [25, 26] and subsequently generalized by Demasi (GUF) [27–29]. The dimensional reduction is carried out within the framework of two variational statements: the classical displacement-based approach expressed by the Principle of Virtual Displacements (PVD), and the mixed approach proposed by Reissner and referred to as Reissner Mixed Variational Theorem (RMVT) [30, 31]. RMVT allows to introduce independent assumptions for the field variables requiring to be interlaminar continuous, i.e., the displacements and the transverse stresses, thus permitting the model to *a priori* fulfil the so-called “ C_z^0 –Requirements” [32]. Axiomatic *variable kinematics* models are then constructed that can adopt *Equivalent Single Layer* (ESL) as well as *Layer-Wise* (LW) descriptions for the field variables.

Zig-Zag Theories (ZZT) are a special class of ESL models towards meeting the C_z^0 -Requirements. We refer to [33] for a comprehensive and clear historical review of ZZT.

Among the different approaches developed over the last decades, CUF adopts the simple Zig-Zag Function proposed by Murakami [34]. More recently, the Refined Zig-Zag Theory (RZT) has been proposed for composite plates [35] and subsequently enhanced by referring to RMVT [36]. Thorough comparisons between MZZF and RZT can be found in [37, 38].

By virtue of the Unified Formulation, these models are expressed in a compact index notation that enables their implementation in terms of *kernel arrays* or *fundamental nuclei*. As a result, the user can select the model to be employed in the analysis at runtime, thus depending on the desired accuracy and intended output. Since the most refined models of CUF and GUF are capable of furnishing quasi-3D solutions, see, e.g., [39], the error introduced by a given model with respect to a certain output quantity can be quantitatively assessed, hence allowing to resolve the problem-dependent accuracy issue by resorting to an Axiomatic/Asymptotic Method [40–43].

D’Ottavio formally extended GUF upon enabling the possibility of selecting different models for individual Sublaminates (SGUF), which consist of an arbitrary number of contiguous plies within the composite stack [44]. The resulting mixed ESL/LW description is particularly meaningful for sandwich panels, for which different models can be adopted for the thin and stiff skins and the thick and compliant core layers [45]. Therefore, this feature allows to further optimise the number of unknown functions of the structural model without affecting the accuracy. SGUF has been successfully employed in the framework of a Ritz solution method to the analysis of bending, vibration and buckling of sandwich plates and shells, which could comprise multiple cores also [46–49].

This paper presents for the first time the Finite Element (FE) implementation of SGUF variable kinematics plate models. Both PVD- and mixed RMVT-based element formulations are considered. Bi-linear four-node elements based on refined shear-deformable plate models suffer the same well-known transverse shear locking problem affecting FSDT. In order to avoid the drawbacks of the reduced-order quadrature technique, recent FE implementations of variable kinematics models have been proposed which adopt the MITC4 approach [50, 51]. The ANS approach has been used to formulate robust 4-node quadrilateral FEs for ESL and LW shell models based on a refined through-thickness kinematics expressed in a Sampling-Surfaces description using Lagrange polynomials [52–54]. A robust four-nodes quadrilateral plate element is formulated based on previous FE developments dedicated to CUF models [55, 56]. Also, it is shown for the first time that the local stress response can be improved by prescribing values for the transverse stress degrees-of-freedom (DOF) of RMVT-based variable kinematics elements.

The paper is organised as follows. The variable kinematics approach of SGUF is briefly recalled in Section 2 and the FE interpolations along with the resulting algebraic governing equations for the linear statics problem are given in Section 3. The results discussed in Section 4 are entirely dedicated to sandwich plate applications and allow to appreciate the robustness and versatility of the developed computational approach, which is capable of attaining quasi-3D solutions with simple 2D meshes even in problems involving localised core indentations. Finally, conclusions are summarized and further works outlined in Section 5.

2 Variable kinematics plate model

2.1 Geometry description

Let us consider a multilayered rectangular plate of total thickness h , composed of N_p orthotropic, elastic and perfectly bonded plies occupying the volume $V = \Omega \times \{-h/2 \leq x_3 \leq h/2\}$ in the Cartesian frame $(x_1, x_2, x_3 \equiv z)$, see Fig. 1 (left). The reference surface Ω is thus chosen to lie in the plate midplane ($z = 0$). The boundary ∂V is split in the portion ∂V_u with an imposed displacement field \bar{u}_i and ∂V_t with imposed tractions \bar{t}_i such that $\partial V_u \cup \partial V_t = V$ and $\partial V_u \cap \partial V_t = \emptyset$. Unless differently stated, the Einstein summation convention is employed with Latin indices varying in $\{1, 2, 3\}$ and Greek indices in $\{1, 2\}$. The composite cross-section is shown in Fig. 1 (right), where $p = 1, 2 \dots N_p$ is the index for the physical plies and $k = 1, 2 \dots N_l$ is the index for the numerical layers in which the laminate is subdivided into. The number of physical plies composing the k^{th} numerical layer is indicated as N_p^k . Non-dimensional coordinates $\zeta_k \in \{-1, 1\}$ and $\zeta_p \in \{-1, 1\}$ are introduced in order to define the interpolations across the thickness of the k^{th} layer and the p^{th} ply, respectively:

$$\zeta_{\square} = \frac{2}{h_{\square}} z - \frac{z_t^{\square} + z_b^{\square}}{z_t^{\square} - z_b^{\square}} \quad \text{with} \quad \square = p, k \quad (1)$$

where $h_k = z_t^k - z_b^k$ and $h_p = z_t^p - z_b^p$ denotes the layer and ply thickness, respectively. The relation between the non-dimensional ply-specific and layer-specific coordinates is obtained as:

$$\zeta_p = \frac{h_k}{h_p} \zeta_k + \frac{2}{h_p} (z_{0_k} - z_{0_p}) = \frac{2}{\zeta_k^{p,t} - \zeta_k^{p,b}} \left(\zeta_k - \frac{\zeta_k^{p,t} + \zeta_k^{p,b}}{2} \right) \quad (2)$$

where $z_{0_{\square}} = (z_t^{\square} + z_b^{\square})/2$ are the mid-plane coordinates of the k^{th} layer ($\square = k$) and the p^{th} ply ($\square = p$), respectively. Finally, $\zeta_k^{p,t}$ and $\zeta_k^{p,b}$ are the values of the non-dimensional coordinate ζ_k at the top and bottom interfaces, respectively, of the physical ply p inside the k^{th} sublaminates, i.e., $\zeta_p(\zeta_k = \zeta_k^{p,t}) = 1$ and $\zeta_p(\zeta_k = \zeta_k^{p,b}) = -1$.

2.2 Variational formulations

Variational formulations are used to introduce the axiomatic modeling along the thickness coordinate and the FE approximations over the reference surface Ω . The conventional displacement-based approach (PVD) as well as the mixed approach by Reissner (RMVT) will be employed for deriving the governing equations of the composite plate. In either case, the governing equations are expressed by equating the internal virtual work with the virtual work done by the external tractions \bar{t}_i :

$$\delta W_{int} = \delta W_{ext} \quad \text{with} \quad \delta W_{ext} = \int_{\partial V_t} \delta u_i \bar{t}_i \, d\Gamma \quad (3)$$

where δ is the usual variational operator and u_i the displacement vector field. Invoking the assumption of small perturbations, the attention is restricted to the classical linear elasticity with small displacements and strains.

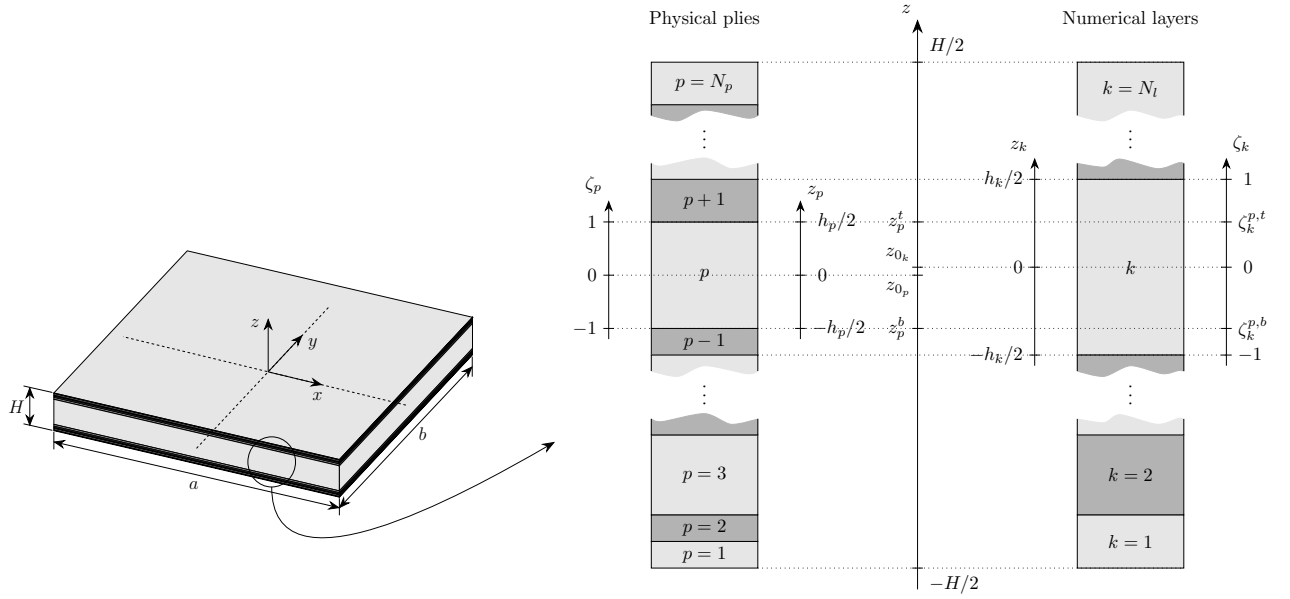


Figure 1: Multilayered plate as an assembly of N_p physical plies (left) and N_l numerical layers (right). Global z , layer-specific z_k and ply-specific z_p coordinates are introduced along with the non-dimensional layer- and ply-specific coordinates ζ_k and ζ_p .

2.2.1 The Principle of Virtual Displacement (PVD)

The PVD yields the weak form of the equilibrium equations under the assumption of a compatible kinematic field and the verification of the constitutive law. The strain and stress fields are split into their in-plane (subscript b), transverse normal (subscript n) and transverse shear (subscript s) components as

$$\begin{aligned}
 \boldsymbol{\epsilon}_b &= [\epsilon_{xx} \ \epsilon_{yy} \ \gamma_{xy}]^T; & \epsilon_n &= \epsilon_{zz}; & \boldsymbol{\epsilon}_s &= [\gamma_{yz} \ \gamma_{xz}]^T \\
 \boldsymbol{\sigma}_b &= [\sigma_{xx} \ \sigma_{yy} \ \sigma_{xy}]^T; & \sigma_n &= \sigma_{zz}; & \boldsymbol{\sigma}_s &= [\sigma_{xz} \ \sigma_{yz}]^T
 \end{aligned} \tag{4}$$

where $\gamma_{ij} = 2\epsilon_{ij}$ ($i \neq j$) and superscript T indicates the transposition operation. Referring to the contracted vector notation for the symmetric strain and stress tensors, the constitutive link for each physical ply p is expressed in matrix form in the Cartesian frame (x, y, z) as

$$\begin{bmatrix} \boldsymbol{\sigma}_b \\ \sigma_n \\ \boldsymbol{\sigma}_s \end{bmatrix}^{(p)} = \begin{bmatrix} \tilde{\mathbf{C}}_{bb} & \tilde{\mathbf{C}}_{bn} & 0 \\ \tilde{\mathbf{C}}_{bn}^T & \tilde{\mathbf{C}}_{nn} & 0 \\ 0 & 0 & \tilde{\mathbf{C}}_{ss} \end{bmatrix}^{(p)} \begin{bmatrix} \boldsymbol{\epsilon}_b \\ \epsilon_n \\ \boldsymbol{\epsilon}_s \end{bmatrix}^{(p)} \tag{5}$$

in which the stiffness coefficients $\tilde{\mathbf{C}}$ of the orthotropic ply are expressed in the plate's Cartesian frame through a rotation angle θ_p about the z -axis [57]. The virtual internal work for the

PVD is expressed by the following integral

$$\begin{aligned}
\delta W_{int} &= \int_V \delta \boldsymbol{\epsilon}_b^T \boldsymbol{\sigma}_b + \delta \boldsymbol{\epsilon}_n^T \boldsymbol{\sigma}_n + \delta \boldsymbol{\epsilon}_s^T \boldsymbol{\sigma}_s \, dV = \\
&= \int_\Omega \sum_{p=1}^{N_p} \int_{h_p} \left\{ \delta \boldsymbol{\epsilon}_b^{(p)T} \tilde{\mathbf{C}}_{bb}^{(p)} \boldsymbol{\epsilon}_b^{(p)} + \delta \boldsymbol{\epsilon}_b^{(p)T} \tilde{\mathbf{C}}_{bn}^{(p)} \boldsymbol{\epsilon}_n^{(p)} + \delta \boldsymbol{\epsilon}_n^{(p)T} \tilde{\mathbf{C}}_{bn}^{(p)T} \boldsymbol{\epsilon}_b^{(p)} + \delta \boldsymbol{\epsilon}_n^{(p)T} \tilde{\mathbf{C}}_{nn}^{(p)} \boldsymbol{\epsilon}_n^{(p)} \right. \\
&\quad \left. + \left\{ \delta \boldsymbol{\epsilon}_s^{(p)T} \tilde{\mathbf{C}}_{ss}^{(p)} \boldsymbol{\epsilon}_s^{(p)} \, dz \right\} \, dx \, dy \right. \quad (6)
\end{aligned}$$

2.2.2 The Reissner Mixed Variational Theorem (RMVT)

RMVT allows to introduce independent approximations for the transverse stress field in view of an *a priori* fulfilment of the interlaminar equilibrium [30, 31]. The virtual internal work for RMVT can be written as

$$\begin{aligned}
\delta W_{int} &= \int_V \delta \boldsymbol{\epsilon}_b^T \boldsymbol{\sigma}_b + \delta \epsilon_n \sigma_n + \delta \boldsymbol{\epsilon}_s^T \boldsymbol{\sigma}_s + \delta \sigma_n^T (\epsilon_n - e_n) + \delta \boldsymbol{\sigma}_s^T (\boldsymbol{\epsilon}_s - \boldsymbol{e}_s) \, dV \\
&= \int_\Omega \sum_{p=1}^{N_p} \int_{h_p} \left\{ \delta \boldsymbol{\epsilon}_b^{(p)T} \mathbf{C}_{bb}^{(p)} \boldsymbol{\epsilon}_b^{(p)} + \delta \boldsymbol{\epsilon}_b^{(p)T} \mathbf{C}_{bn}^{(p)} \sigma_n^{(p)} + \delta \epsilon_n^{(p)T} \sigma_n^{(p)} + \delta \boldsymbol{\epsilon}_s^{(p)T} \boldsymbol{\sigma}_s^{(p)} + \delta \sigma_n^{(p)T} \epsilon_n^{(p)} \right. \\
&\quad \left. + \delta \sigma_n^{(p)T} \mathbf{C}_{bn}^{(p)T} \boldsymbol{\epsilon}_b^{(p)} - \delta \sigma_n^{(p)T} C_{nn} \sigma_n^{(p)} + \delta \boldsymbol{\sigma}_s^{(p)T} \boldsymbol{\epsilon}_s^{(p)} - \delta \boldsymbol{\sigma}_s^{(p)T} \mathbf{C}_{ss}^{(p)} \boldsymbol{\sigma}_s^{(p)} \, dz \right\} \, dx \, dy \quad (7)
\end{aligned}$$

in which the following definitions have been used for the in-plane stresses $\boldsymbol{\sigma}_b$ and the transverse strains $\boldsymbol{e} = [e_n \, \boldsymbol{e}_s]^T$ in each ply p :

$$\begin{bmatrix} \boldsymbol{\sigma}_b \\ e_n \\ \boldsymbol{e}_s \end{bmatrix}^{(p)} = \begin{bmatrix} \mathbf{C}_{bb} & \mathbf{C}_{bn} & 0 \\ -\mathbf{C}_{bn}^T & C_{nn} & 0 \\ 0 & 0 & \mathbf{C}_{ss} \end{bmatrix}^{(p)} \begin{bmatrix} \boldsymbol{\epsilon}_b \\ \sigma_n \\ \boldsymbol{\sigma}_s \end{bmatrix}^{(p)} \quad (8)$$

where the coefficients of this *mixed form* of constitutive law are related to those of Hooke's law Eq. (5) by

$$\mathbf{C}_{bb} = \tilde{\mathbf{C}}_{bb} + \tilde{\mathbf{C}}_{bn} \tilde{\mathbf{C}}_{nn}^{-1} \tilde{\mathbf{C}}_{bn}^T; \quad \mathbf{C}_{bn} = \tilde{\mathbf{C}}_{bn} \tilde{\mathbf{C}}_{nn}^{-1}; \quad C_{nn} = \tilde{C}_{nn}^{-1}; \quad \mathbf{C}_{ss} = \tilde{\mathbf{C}}_{ss}^{-1} \quad (9)$$

2.3 Variable-kinematics plate model in SGUF

The plate model is defined upon introducing *ad hoc* assumptions for the distribution across the thickness of the generic dependent variable \mathcal{U} of the variational framework to be used, i.e., $\mathcal{U} \in \{u_i\}$ for a PVD model and $\mathcal{U} \in \{u_i, \sigma_{i3}\}$ for an RMVT model. The assumptions are expressed in each sublaminar k and *independently for each variable \mathcal{U}^k* according to the GUF notation [44] as follows

$$\mathcal{U}^k(x, y, z_k) = \sum_{\alpha_{\mathcal{U}}=0}^{N_{\mathcal{U}}^k} F_{\alpha_{\mathcal{U}}}(\zeta) \hat{\mathcal{U}}_{\alpha_{\mathcal{U}}}^k(x, y) \quad (10)$$

In each sublaminar, the generic variable \mathcal{U}^k can be described either in an ESL sense by setting $\zeta = \zeta_k$, or in a LW sense by setting $\zeta = \zeta_p$. In this latter case, the approximation is

defined as the assembly all N_p^k ply-specific contributions:

$$\mathcal{U}^k(x, y, z_k) = \sum_{p=1}^{N_p^k} \mathcal{U}^{(p)}(x, y, z_p) = \sum_{p=1}^{N_p^k} \sum_{\alpha_{\mathcal{U}}=0}^{N_{\mathcal{U}}^k} F_{\alpha_{\mathcal{U}}}(\zeta_p) \hat{\mathcal{U}}_{\alpha_{\mathcal{U}}}^{(p)}(x, y) \quad (11)$$

where it is intended that the expansion order $N_{\mathcal{U}}^k$ is the same for all the N_p^k plies within the sublaminate. The model for the whole multilayer is eventually constructed upon assembling in a LW sense all sublaminate-specific contributions.

The thickness functions are defined as

$$F_0(\zeta) = \frac{P_0(\zeta) - P_1(\zeta)}{2}; \quad F_1(\zeta) = \frac{P_0(\zeta) + P_1(\zeta)}{2}; \quad F_r(\zeta) = P_r(\zeta) - P_{r-2}(\zeta) \text{ for } r \geq 2 \quad (12)$$

where $P_m(\zeta)$ is the Legendre polynomial of order m :

$$P_0 = 1; \quad P_1 = \zeta; \quad P_{n+1} = \frac{(2n+1)\zeta P_n - nP_{n-1}}{n+1} \quad (13)$$

This hierarchic basis is used for both, the ESL and LW descriptions of the variable inside a sublaminate. In the ESL case one sets $\zeta = \zeta_k$, whereas $\zeta = \zeta_p$ is used for a LW description.

The assembly procedures of LW contributions is carried out by imposing the interlaminar continuity of the variable \mathcal{U} , i.e., by stating the perfect bond condition of adjacent plies and sublaminates. By virtue of the property $F_0(-1) = F_1(1) = 1, F_r(\pm 1) = 0$, it is straightforward to enforce the continuity within a classical assembly procedure, see [44] for more details.

2.4 The semi-discrete governing equations of the plate

The approximations across the thickness, expressed in the compact notation Eq. (11), are introduced into the virtual work integral Eq. (6) (PVD) or Eq. (7) (RMVT). As a result, the virtual internal work defined by the generic unknown variable \mathcal{U}_s and the virtual variation $\delta\mathcal{U}_q$ can be expressed as

$$\delta W_{int}(\delta\hat{\mathcal{U}}_q(x, y), \hat{\mathcal{U}}_s(x, y)) = \sum_{k=1}^{N_l} \sum_{p=1}^{N_p^k} \delta W_{int}^{(p)}(\delta\hat{\mathcal{U}}_q^{(p)}(x, y), \hat{\mathcal{U}}_s^{(p)}(x, y)) \quad (14)$$

where the contribution of the p^{th} ply of the k^{th} sublaminate can be written as follows:

$$\delta W_{int}^{(p)}(\delta\hat{\mathcal{U}}_q^{(p)}, \hat{\mathcal{U}}_s^{(p)}) = \int_{\Omega} \left(\partial_{\alpha}^q [\delta\hat{\mathcal{U}}_{q\mu_q}^{(p)}(x, y)] \right) Z_{\partial_z^q \mathcal{U}_q \partial_z^s \mathcal{U}_s}^{p\mu_q \tau_{\mathcal{U}_s} mn} \left(\partial_{\beta}^s [\hat{\mathcal{U}}_{s\tau_s}^{(p)}(x, y)] \right) dx dy \quad (15)$$

The operators $\partial_{\alpha}^q[\cdot]$ and $\partial_{\beta}^s[\cdot]$ indicate that the variables $\hat{\mathcal{U}}_s$ and $\delta\hat{\mathcal{U}}_q$ may be partially derived with respect to the in-plane coordinates, depending on the strain component involved in the specific virtual work contribution being considered. Furthermore, the thickness integral Z has been introduced as

$$Z_{\partial_z^q \mathcal{U}_q \partial_z^s \mathcal{U}_s}^{p\mu_q \tau_{\mathcal{U}_s} mn} = \int_{h_p} \left(\partial_z^q [F_{\mu_q}^m(\zeta_p)] \right) c_{QS}^p \left(\partial_z^s [F_{\tau_s}^n(\zeta_p)] \right) dz \quad (16)$$

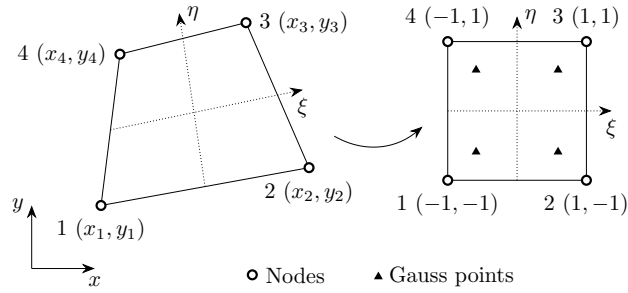


Figure 2: Four-node quadrangular element in the physical Cartesian frame (x, y) and in the natural frame (ξ, η) .

Again, $\partial_z [\cdot]$ indicates that a derivation with respect to the thickness coordinate z may be required for defining the strain component pertaining to the specific contribution to the virtual work. As it will become clear when introducing the finite element interpolations (Section 3.1), thickness functions could be split in their z -constant part and the higher-order part that depends on powers of z ; this is taken into account by the superscripts m and n (with $m, n \in \{0, h, a\}$, where a means that both contributions are to be included). The coefficient c_{QS}^p can represent a material parameter (with $Q, S \in \{1, 6\}$), or a unitary coefficient, because in RMVT the compatible transverse strains are directly work-conjugated to the transverse stress variables. Note also that in RMVT transverse stress variables are never derived with respect to any coordinate.

Eq. (15) is the generic expression of the model-invariant *kernel* of the semi-discrete stiffness matrix, which is computed upon cycling over all indices q, μ_q, s, τ_s and subsequently assembled over all plies p and sublaminates k . Specific instances of the *kernels* are formed by expressing all individual virtual work contributions pertaining to the model: PVD-based models rely on 6 *kernels*, whereas RMVT-based models require 15 *kernels*.

The thickness integrals are explicitly carried out and assembled across the whole multilayer section, which yields the dimensionally reduced 2D model. The strong form of the 2D governing equations, obtained upon integration by parts of those terms subjected to the derivative ∂_α^q , have been given in [44] and solved in the framework of the Navier solution. Weak-form solutions have been addressed in [46] by referring to the Ritz method. In this paper, the Finite Element Method is for the first time used to obtain weak-form solutions of SGUF models.

3 Finite Element Formulation

The solution over the reference surface Ω is discretized through four-node quadrilateral elements, see Fig. 2.

The classical C_0^0 isoparametric interpolation is employed for all variables (i.e., displacement variables for PVD, and displacement and transverse stress variables for RMVT). However, in order to circumvent the well-known transverse shear locking pathology, the dedicated field-compatible approximation named QC4 is used to substitute the isoparametric interpolation for the transverse shear strain $\gamma_{\alpha 3}$ [55].

3.1 Strain-displacement relations

The development of FEs for the QC4 interpolation requires a new definition of the strain field. In particular, only the z -constant part of the transverse shear strain field $\gamma_{\alpha 3}^0$ is responsible for the locking pathology, because high-order terms $\gamma_{\alpha 3}^h$ that depend on powers > 1 of the thickness coordinate z naturally vanish as the plate becomes thin. Therefore, the substitute interpolation will be used only for the field $\gamma_{\alpha 3}^0$, which is carried out by opportunely selecting the z -independent terms of the thickness expansion. By introducing the compact index notation, $\mathbf{U}_{\mu\mathcal{U}}^{(k)}$ is the displacement DOF vector related to the i^{th} node ($i \in \{1, 4\}$), the k^{th} layer and the expansion order index $\mu\mathcal{U}$:

$$\mathbf{U}_{\mu\mathcal{U}}^{(k)} = \left[U_{x\mu u_x}^{(k)} \quad U_{y\mu u_y}^{(k)} \quad U_{z\mu u_z}^{(k)} \right]_i^T \quad (17)$$

The geometrical relations that define the discretized strain field can be then expressed in the following matrix notation:

$$\begin{aligned} \boldsymbol{\epsilon}_b^{(k)}(x, y, z_p) &= \mathbf{F}_{b\mu\mathcal{U}}(z_p) \mathbf{B}_{bi}(x, y) \mathbf{U}_{\mu\mathcal{U}}^{(k)} \\ \epsilon_n^{(k)}(x, y, z_p) &= \mathbf{F}_{n\mu\mathcal{U}}(z_p) \mathbf{B}_{ni}(x, y) \mathbf{U}_{\mu\mathcal{U}}^{(k)} \\ \boldsymbol{\epsilon}_s^{(k)}(x, y, z_p) &= \boldsymbol{\gamma}^0(x, y) + \boldsymbol{\gamma}^h(x, y, z_p) \\ &= \mathbf{F}_{s\mu\mathcal{U}}^0 \bar{\mathbf{B}}_{si}(x, y) \mathbf{U}_{\mu\mathcal{U}}^{(k)} + \mathbf{F}_{s\mu\mathcal{U}}^h(z_p) \mathbf{B}_{si}(x, y) \mathbf{U}_{\mu\mathcal{U}}^{(k)} \end{aligned} \quad (18)$$

where the \mathbf{B} matrices contain the derivatives of the isoparametric shape functions that define the in-plane strains (subscript b), the transverse normal strain (subscript n) and the transverse shear strains (subscript s). The substitute interpolation for the z -constant part of the transverse shear strain is indicated by the $\bar{\mathbf{B}}_s$ matrix. For the QC4 interpolation, the matrix of the thickness functions $\mathbf{F}_{s\mu\mathcal{U}}$ must be split into the z -constant part $\mathbf{F}_{s\mu\mathcal{U}}^0$ and the part $\mathbf{F}_{s\mu\mathcal{U}}^h$ that depends on z . The interpolation scheme involved in the definition of the z -constant component $\boldsymbol{\gamma}^0$ of the transverse shear strain field is detailed in Appendix B.

The explicit expressions for the matrices containing the through-thickness functions ($\mathbf{F}_{b\mu\mathcal{U}}$, $\mathbf{F}_{n\mu\mathcal{U}}$, $\mathbf{F}_{s\mu\mathcal{U}}^0$ and $\mathbf{F}_{s\mu\mathcal{U}}^h$) as well as those containing the in-plane derivatives of the FE shape functions (\mathbf{B}_{bi} , \mathbf{B}_{ni} , $\bar{\mathbf{B}}_{si}$ and \mathbf{B}_{si}) are given in Appendix A.

Finally, it is worth highlighting that the QC4 interpolation is defined in the natural element frame, which enhances the FE accuracy in presence of distorted mesh. This is carried out by accounting for the Jacobian matrix \mathbf{J} evaluated at Gauss points in the definition of $\boldsymbol{\gamma}^0$.

3.2 FE matrices

The governing equations for both PVD-based and RMVT-based formulations are finally derived by substituting the strain-displacement relations Eq. (18) in the corresponding weak forms expressed by Eq. (6) and Eq. (7), along with the opportune constitutive law (Eq. (5), Eq. (8)).

The following algebraic systems are eventually obtained, in which the nodal unknowns are the through-thickness parameters defining the displacement field and, for the RMVT approach, the transverse stress field:

$$\text{PVD: } \begin{bmatrix} \mathbf{K}_{u_x u_x} & \mathbf{K}_{u_x u_y} & \mathbf{K}_{u_x u_z} \\ & \mathbf{K}_{u_y u_y} & \mathbf{K}_{u_y u_z} \\ \text{sym} & & \mathbf{K}_{u_z u_z} \end{bmatrix} \begin{bmatrix} \mathbf{U}_x \\ \mathbf{U}_y \\ \mathbf{U}_z \end{bmatrix} = \begin{bmatrix} \mathbf{R}_x \\ \mathbf{R}_y \\ \mathbf{R}_z \end{bmatrix} \quad (19)$$

$$\text{RMVT: } \begin{bmatrix} \mathbf{K}_{u_x u_x} & \mathbf{K}_{u_x u_y} & \mathbf{0}_{u_x u_z} & \mathbf{K}_{u_x s_x} & \mathbf{K}_{u_x s_y} & \mathbf{K}_{u_x s_z} \\ & \mathbf{K}_{u_y u_y} & \mathbf{0}_{u_y u_z} & \mathbf{K}_{u_y s_x} & \mathbf{K}_{u_y s_y} & \mathbf{K}_{u_y s_z} \\ & & \mathbf{0}_{u_z u_z} & \mathbf{K}_{u_z s_x} & \mathbf{K}_{u_z s_y} & \mathbf{K}_{u_z s_z} \\ & & & \mathbf{K}_{s_x s_x} & \mathbf{K}_{s_x s_y} & \mathbf{0}_{s_x s_z} \\ \text{sym} & & & & \mathbf{K}_{s_y s_y} & \mathbf{0}_{s_y s_z} \\ & & & & & \mathbf{K}_{s_z s_z} \end{bmatrix} \begin{bmatrix} \mathbf{U}_x \\ \mathbf{U}_y \\ \mathbf{U}_z \\ \mathbf{S}_x \\ \mathbf{S}_y \\ \mathbf{S}_z \end{bmatrix} = \begin{bmatrix} \mathbf{R}_x \\ \mathbf{R}_y \\ \mathbf{R}_z \\ \mathbf{0} \\ \mathbf{0} \\ \mathbf{0} \end{bmatrix} \quad (20)$$

It worth emphasising that, in contrast to the algebraic systems of the RMVT formulation obtained in the framework of Navier's strong form solution or Ritz' weak form solutions, the coupling terms $\mathbf{K}_{u_x s_y}$ and $\mathbf{K}_{u_y s_x}$ are non-zero due to the QC4 interpolation scheme. All *kernels* from which the contributions of the stiffness matrices are obtained through opportune cycling over the various indices are explicitly expressed in Appendix C.

4 Numerical results

The developed 4-node FE for variable kinematics SGUF models is here applied to the static response sandwich plates. Three problems are considered. The global bending of a simply-supported square plate, for which Kardomateas provided exact elasticity solutions [58], is used for displaying the convergence properties of the FE and for a first assessment of PVD-based and RMVT-based SGUF models. The rectangular sandwich plate subjected to a localized pressure proposed by Meyer-Piening [59] is a more challenging problem due to the steep gradients produced by the local load. Finally, a typical indentation problem of a sandwich beam under a point force is examined, as considered in, e.g., [60–63]. The considered problems aim at displaying the robustness of the numerical FE-based tool and the flexibility of the variable kinematics modeling approach of SGUF, in particular its capability of recovering accurate through-thickness response with a simple 2D mesh.

4.1 Employed models and acronyms

SGUF models for the sandwich plates are specified by the GUF-type model employed for the facesheets and the core separated by a slash, see also [44]. The meaning of the models' acronyms is recalled in Fig. 3. Displacement-based models with a z -constant out-of-plane displacement ($N_{u_3} = 0$) resort to the reduced plane-stress constitutive coefficients. The plane stress assumption $\sigma_{33} = 0$ is represented in RMVT-models by dropping off the σ_{33} variable, which is indicated in the acronym by replacing the expansion order N_{s_3} by a dot (\cdot). Simplified CUF-type acronyms are used if the same description (ESL or LW) and expansion order N is used for *all* variables, e.g., $D_{Z_2 Z_2} = \text{EDZ2}$, $M_{L_7 L_7}^{L_7 L_7} = \text{LM7}$, $M_{Z_4 Z_4}^{E_4 E_4} = \text{EMZ4}$ etc. FSDT is thus obtained as ED_{10} , and CLT is obtained from FSDT by numerically penalizing the transverse shear stiffness.

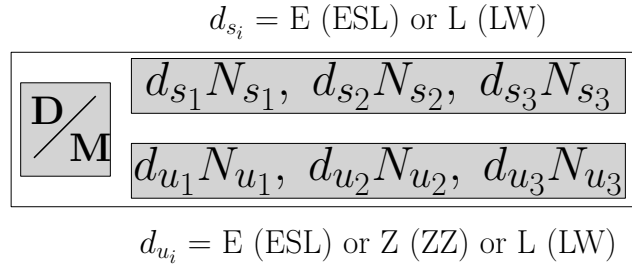


Figure 3: Structure of the acronyms for the considered GUF-type models

Some additional features are here introduced for the first time concerning the approximations of the transverse stresses in RMVT-based models. In particular, prescribed zero values can be enforced as homogeneous boundary conditions for the transverse shear stresses. This can be done across the thickness at the top and/or bottom surfaces $z = \pm \frac{H}{2}$ as well as in the (x, y) -plane at the nodal DOF of the FE. In order to indicate the exact satisfaction of the homogeneous boundary conditions for the transverse shear stress at the plates' top and bottom surfaces, the symbol \bullet is appended after the expansion order, e.g., EM_{10}^{\bullet} is a refined FSDT that retains a quadratic transverse shear stress satisfying the homogeneous conditions $\sigma_{\alpha 3}(x, y, \pm \frac{H}{2}) = 0$. It is emphasized that homogeneous transverse stresses are enforced only in mixed models based on RMVT in order to avoid the static inconsistencies that may plague high-order PVD-based models [64].

4.2 Kardomateas sandwich plate

The elasticity solution proposed by Pagano in [65] has been extended by Kardomateas towards more realistic core materials, in particular transversely isotropic cores that are stiffer in the transverse direction than in the in-plane directions, e.g., honeycomb cores [66]. The Kardomateas-TestCase (K-TC) considers a simply-supported square three-layered sandwich panel subjected to a bi-sinusoidal pressure load, see Fig. 4, with Graphite/Epoxy unidirectional faces and a glass-phenolic honeycomb core. The geometry and material data are listed in Tab. 1.

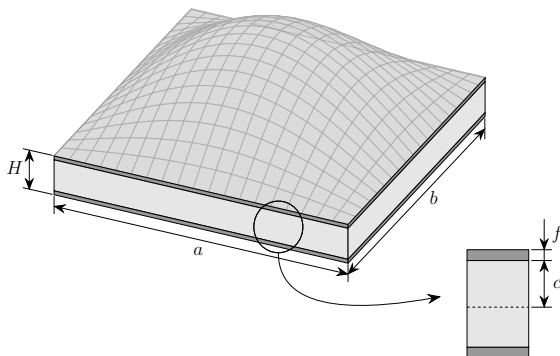


Figure 4: K-TC: Bi-sinusoidal pressure at top surface.

Table 1: K-TC: Sandwich plate geometry and material data

$a = b = 10H; f = 2 \text{ mm}; 2c = 16 \text{ mm}$		
	T300/5208 Graphite/Epoxy	Glass-phenolic honeycomb
E_{11} [GPa]	181	0.032
E_{22} [GPa]	10.3	0.032
E_{33} [GPa]	10.3	0.3
ν_{12}	0.277	0.25
ν_{13}	0.277	0.027
ν_{23}	0.4	0.027
G_{12} [GPa]	7.17	13
G_{13} [GPa]	7.17	48
G_{23} [GPa]	5.96	48

The results are evaluated in terms of the following non-dimensional local response param-

eters:

$$\begin{aligned}
\bar{U}(z) &= u_x(-a/2, 0, z) \frac{E_{11}}{q_0 H S^3}; & \bar{V}(z) &= u_y(0, -b/2, z) \frac{E_{11}}{q_0 H S^3}; \\
\bar{W}(z) &= u_z(0, 0, z) \frac{E_{11}}{100 q_0 H}; & \bar{S}_{\alpha\alpha}(z) &= \sigma_{\alpha\alpha}(0, 0, z) \frac{1}{q_0 S^2}; \\
\bar{S}_{xy}(z) &= \sigma_{xy}(-a/2, -b/2, z) \frac{1}{q_0 S^2}; & \bar{S}_{xz}(z) &= \sigma_{xz}(-a/2, 0, z) \frac{1}{q_0 S}; \\
\bar{S}_{yz}(z) &= \sigma_{yz}(0, -b/2, z) \frac{1}{q_0 S}; & \bar{S}_{zz}(z) &= \sigma_{zz}(0, 0, z) \frac{1}{q_0}
\end{aligned} \tag{21}$$

where $S = a/H$ is the plate's length-to-thickness ratio and q_0 the amplitude of the pressure load.

4.2.1 Convergence of the FE

A numerical test is first performed in order to show the convergence of the proposed FE. To this aim, five regular meshes are considered with $N = 2, 4, 8, 16, 32$ four-node elements along the edges of the quarter plate. The convergence analysis is carried out for two representative models, namely the displacement-based FSDT/FSDT and the RMVT-based $EM_{10}^{21}/EM_{32}^{21}$. FE results are compared against the Navier-type closed-form solution for the corresponding model. These results are given in Tab. 2 and labelled by the superscript a .

Table 2: K-TC: Reference values obtained by the Navier-type closed-form solution.

Model	$S = a/H$	$\bar{U}^a(-H/2)$	$\bar{W}^a(H/2)$	$\bar{S}_{xx}^a(H/2)$	$\bar{S}_{xz}^a(0.4H^-)$
FSDT/FSDT	10^1	0.4918643294	230.2174542	1.6339367620	0.2068595369
	10^2	0.3162183647	230729.4323	1.01546741	0.3061014777
	10^3	0.3166019035	2018522809	1.014763335	0.3092905016
$EM_{10}^{21}/EM_{32}^{21}$	10^1	0.4903456822	231.7002615	1.640280194	0.2065009079
	10^2	0.3162178627	230733.5721	1.0154599550	0.3059699424
	10^3	0.3166018998	2018523087	1.0147632530	0.3091640006

The non-dimensional in-plane displacement \bar{U} is evaluated at the bottom of the plate, the transverse displacement \bar{W} and bending stress \bar{S}_{xx} at the top surface and the transverse stress \bar{S}_{xz} at facesheet-core interface. Note that throughout the paper, transverse stresses for PVD-based models are evaluated through the constitutive law.

Convergence curves are reported in Fig. 5 for three different values of the length-to-thickness ratio $S = 10^1, 10^2, 10^3$. For the displacement-based model, the strong locking pathology affecting the fully-integrated isoparametric (ISO4) element is eliminated by resorting to the QC4 interpolation, which thus recovers the asymptotic linear convergence rate. It can be seen that the isoparametric mixed element is much less sensitive to the shear locking: similar results are thus obtained for the RMVT-based ISO4 and QC4 FE, in which the compatible transverse shear strain is interpolated using the substitute interpolation scheme.

Fig. 6 compares the convergence of the RMVT-model for the whole plate to that obtained for the quarter plate ($S = 10$), in which the symmetry conditions are imposed on both

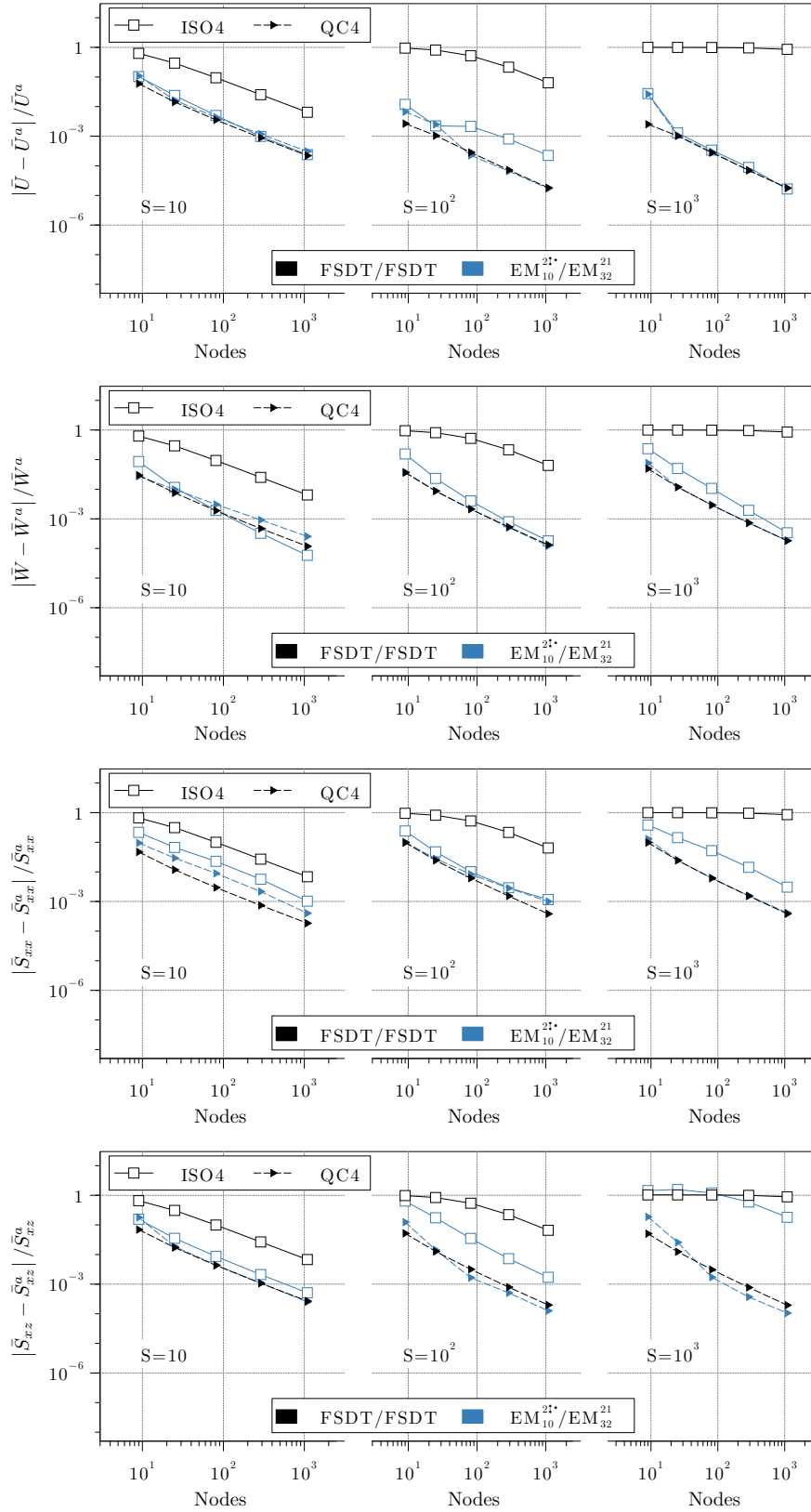


Figure 5: K-TC: Convergence to the Navier-type solution of displacements and stresses of the simply-supported sandwich plate under bi-sinusoidal pressure load for three different values of the length-to-thickness ratio ($S = 10^1, 10^2, 10^3$).

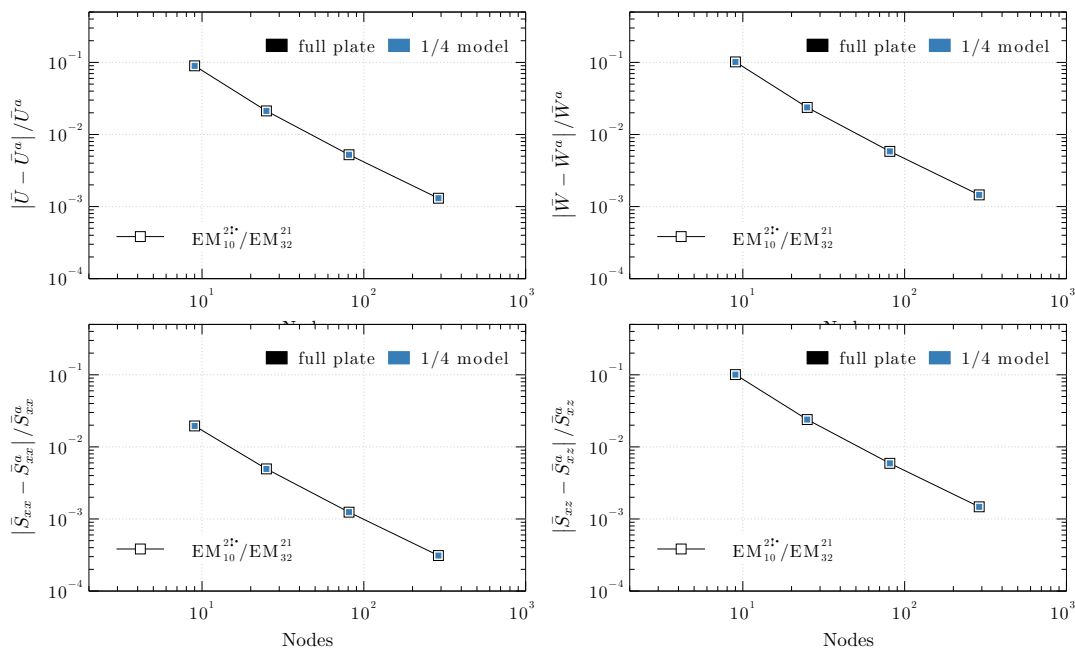


Figure 6: K-TC: Comparison between the convergence for the whole plate case and the quarter plate with symmetry boundary conditions on displacements *and transverse stresses*.

displacement *and transverse stresses*. A perfect match can be appreciated which proves that it is possible to enforce boundary conditions on transverse stress variables on the FE nodes. Results obtained by RMVT models will henceforth verify *a priori* the homogeneity of the transverse shear stresses at the symmetry edges.

4.2.2 Assessment of plate models

The Karamateas benchmark is also used for providing an assessment for several plate theories. The results in Tab. 3 compare the exact 3D solution of [66] with different displacement-based as well as mixed models in terms of through-thickness distributions of the quantities defined in Eq. (21). Based on the previous convergence analysis, a mesh of 16x16 elements is used for a quarter plate and the QC4 interpolation is adopted for the PVD models.

In their comprehensive assessment of PVD models, Carrera and Brischetto [6] have shown that ESL models lead to significant errors for very high skin-to-core stiffness ratios. Tab. 3 shows that RMVT models exhibit the same issue (e.g., EM2). The results also confirm that the use of Murakami's Zig-Zag function (MZZF) improves the accuracy of ESL descriptions for the displacement-based as well as the mixed formulations: it is more important to resolve the slope discontinuity of the displacement field across the facesheet-core interface than to enhance the polynomial order of the approximation.

Table 3: K-TC: Assessment of classical and mixed models. Values in parentheses are the absolute percentage errors with respect to the exact 3D solution.

Model (nDOF)	$\bar{U}(-H/2)$	$\bar{W}(H/2)$	$\bar{S}_{xx}(H/2)$	$\bar{S}_{xz}(0.4H^-)$
Ref [58]	0.4903	231.37	1.6421	0.2064
Displacement-based models				
ED2 (9)	0.3005 (38.71%)	29.812 (87.12%)	0.9719 (40.81%)	0.0089 (95.71%)
ED4 (15)	0.3892 (20.63%)	130.31 (43.68%)	1.2759 (22.30%)	0.0341 (83.48%)
EDZ4 (18)	0.4901 (0.05%)	231.26 (0.05%)	1.6292 (0.78%)	0.2052 (0.55%)
LD4 (39)	0.4908 (0.09%)	231.48 (0.05%)	1.6407 (0.08%)	0.2061 (0.11%)
CLT/FSDT (9)	0.4941 (0.78%)	230.14 (0.53%)	1.6386 (0.21%)	0.2066 (0.11%)
FSDT/FSDT (9)	0.4923 (0.40%)	230.33 (0.45%)	1.6327 (0.57%)	0.2066 (0.13%)
FSDT/ED ₁₂ (11)	0.4909 (0.12%)	231.78 (0.18%)	1.6394 (0.16%)	0.2079 (0.73%)
FSDT/ED ₃₂ (15)	0.4909 (0.12%)	231.78 (0.18%)	1.6394 (0.16%)	0.2063 (0.05%)
Mixed models w/o homogeneous stress BC				
EM2 (18)	0.1809 (63.11%)	158.55 (31.47%)	0.6436 (60.81%)	0.3601 (74.47%)
EM4 (30)	0.4747 (3.19%)	223.95 (3.21%)	1.5893 (3.21%)	0.1522 (26.23%)
EMZ4 (33)	0.4940 (0.74%)	231.96 (0.25%)	1.6512 (0.56%)	0.1858 (9.96%)
LM4 (78)	0.4910 (0.13%)	231.71 (0.15%)	1.6416 (0.03%)	0.2067 (0.15%)
EM ₁₀ ² /EM ₁₀ ⁰ (19)	0.4926 (0.46%)	230.55 (0.35%)	1.6336 (0.51%)	0.2072 (0.38%)
EM ₁₀ ² /EM ₁₀ ² (23)	0.4926 (0.46%)	230.55 (0.35%)	1.6336 (0.51%)	0.2071 (0.36%)
EM ₁₀ ² /EM ₁₂ ⁰¹ (23)	0.4912 (0.17%)	232.01 (0.27%)	1.6403 (0.11%)	0.2071 (0.37%)
EM ₁₀ ² /EM ₃₂ ²¹ (31)	0.4912 (0.17%)	232.01 (0.28%)	1.6404 (0.10%)	0.2068 (0.21%)
Mixed models w/ homogeneous stress BC on $\sigma_{\alpha z}$				
EM ₁₀ ²¹ /EM ₁₀ ⁰ (15)	0.4924 (0.42%)	230.58 (0.34%)	1.6331 (0.55%)	0.2072 (0.38%)
EM ₁₀ ²¹ /EM ₁₀ ² (19)	0.4924 (0.42%)	230.58 (0.34%)	1.6331 (0.55%)	0.2071 (0.34%)
EM ₁₀ ²¹ /EM ₁₂ ⁰¹ (19)	0.4910 (0.14%)	232.03 (0.29%)	1.6397 (0.14%)	0.2071 (0.37%)
EM ₁₀ ²¹ /EM ₃₂ ²¹ (27)	0.4910 (0.13%)	232.04 (0.29%)	1.6398 (0.14%)	0.2068 (0.21%)

The beneficial effect of MZZF is also visible in the distributions displayed in Fig. 7. On the other hand, high order LW models are able to accurately recover the 3D response of the sandwich plate. As it can be appreciated in Fig. 8, the interlaminar discontinuity of the transverse stress field of PVD-based models can be reduced upon increasing the expansion order of the approximation, up to match the *a priori* continuous transverse stress field of RMVT-based models.

Tab. 3 reports results also for several SGUF models, in which one sublaminates is used for each of the facesheets and the core. Thanks to the SGUF approach, the facesheet-core interface can be described in a LW sense and dedicated expansion orders can be used in individual sublaminates: it is hence possible to locally enrich the model for the relatively soft and thick core while keeping simple models for the relatively stiff and thin facesheets, which eventually allows to reduce the number of DOF without affecting the accuracy.

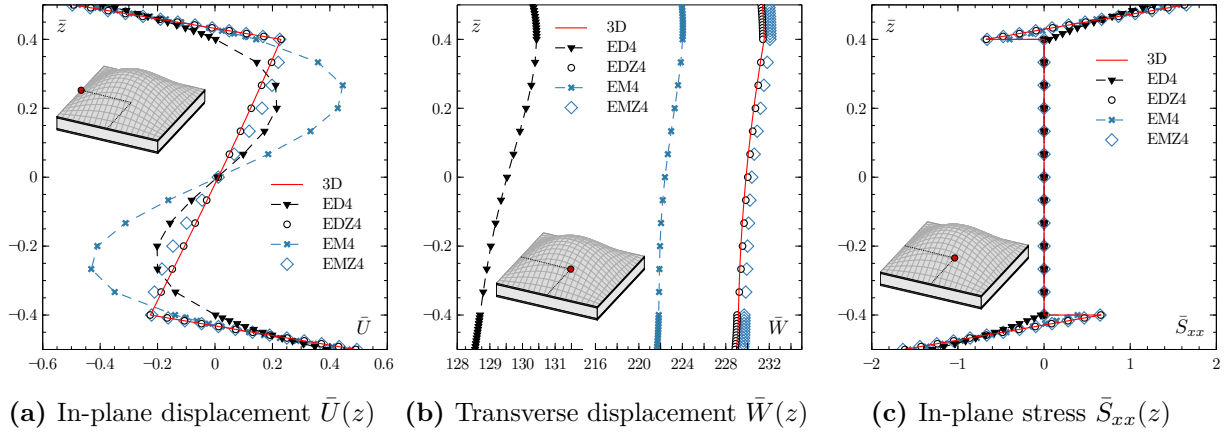


Figure 7: K-TC: Influence of MZZF on Equivalent Single Layer plate theories.

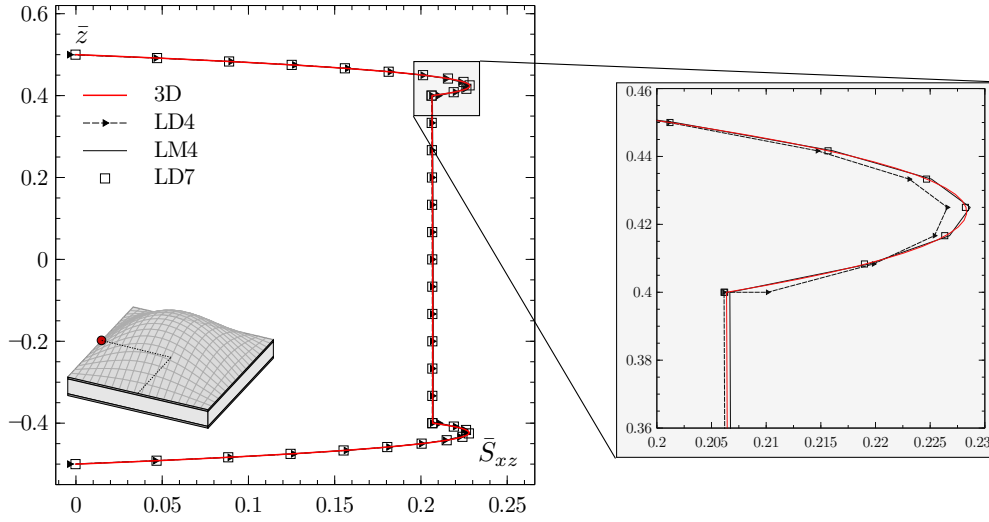


Figure 8: K-TC: Transverse stress \bar{S}_{xz} discontinuity at layer interfaces for displacement-based models.

Furthermore, the through-thickness distributions of PVD-based models are compared against the 3D solution [58] in Fig. 9. The facesheets are modelled according to CLT or FSDT and different kinematics for the core have been investigated, ranging from kinematics invoking the plane-stress constitutive law (FSDT) up to fully 3D models (ED_{12} and ED_{32}). The benefits of an explicit representation of the facesheet-core interfaces are clearly visible: all SGUF models yield errors well below 1%. The advantage is also obvious of enhancing the transverse normal response by locally increasing the expansion order inside the core layer only. Since the transverse normal deformation is mostly confined within the thick core layer, all RMVT models reported in Tab. 3 adopt simple plane-stress models for the facesheets without any substantial accuracy loss. Finally, Fig. 10 compares the through-thickness distribution of the transverse shear stresses \bar{S}_{xz} and \bar{S}_{yz} for the mixed SGUF model EM_{10}^2/EM_{32}^{21} against the equivalent PVD-based model FSDT/ ED_{32} . The accuracy improvement is actually modest unless the homogeneous boundary conditions at the plate's top and bottom surfaces are exactly prescribed: the model EM_{10}^2/EM_{32}^{21} is clearly capable of recovering the exact 3D

solution with 15 displacement DOF and 12 stress DOF per node.

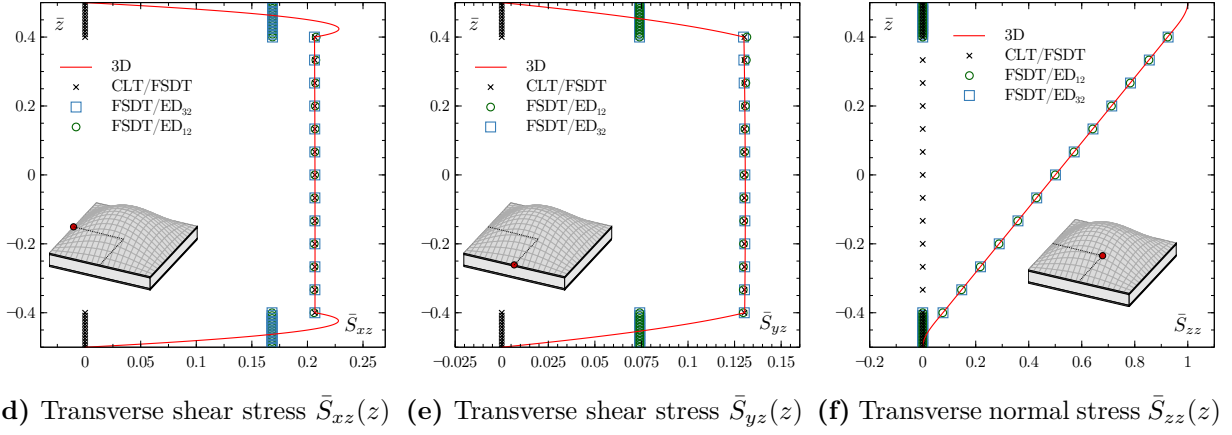
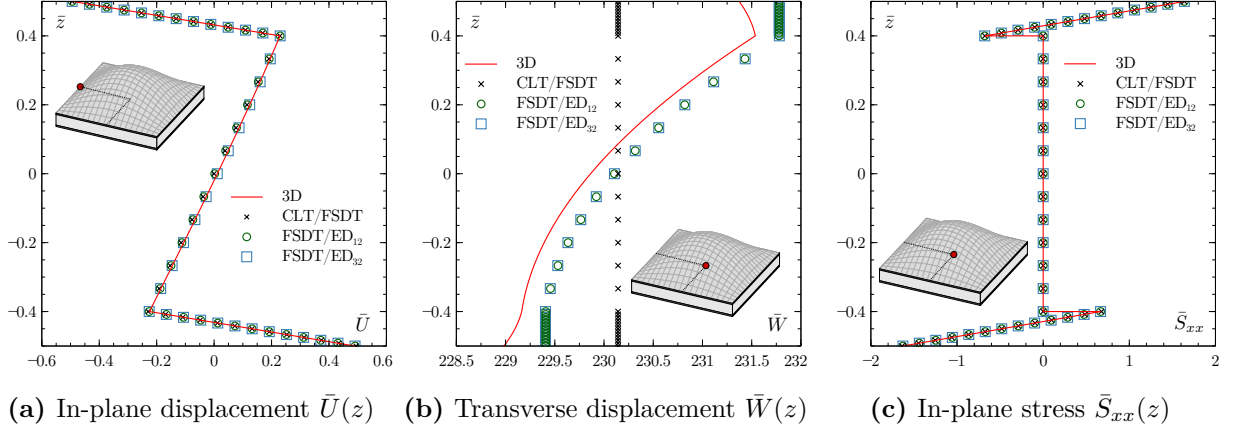


Figure 9: K-TC: Through-thickness distributions of local response parameters for displacement-based SGUF models.

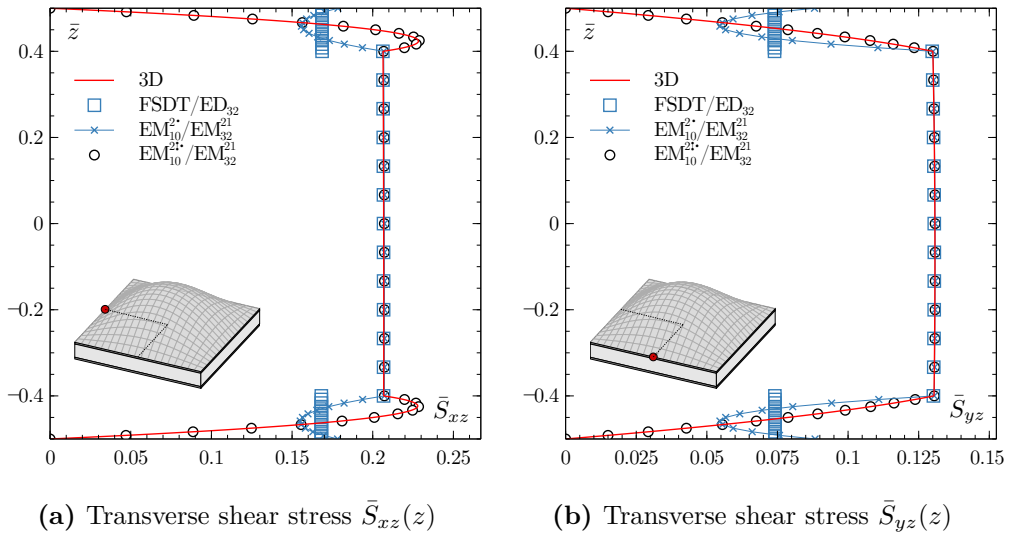


Figure 10: K-TC: Influence of homogenous stress boundary conditions on through-thickness distributions of the transverse shear stresses.

4.3 Meyer-Piening benchmark

The Meyer-Piening TestCase (M-TC) considers a simply supported unsymmetric rectangular plate subjected to a localized transverse pressure [59]. The sandwich plate geometry as well as the elastic properties for the thin facesheets and the core are summarized in Tab. 4. The uniform pressure load $p_0 = 1$ MPa is applied at the top surface on a rectangular area delimited by $x \in [47.5, 52.5]$ mm and by $y \in [90, 110]$ mm, as illustrated in Fig. 11.

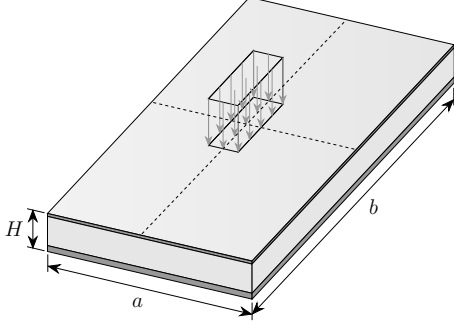


Figure 11: M-TC: Sandwich plate with localized uniform pressure.

Table 4: M-TC: Geometric and material data

$a = 100$ mm; $b = 200$ mm; $H = 12$ mm			
	Lower face	Core	Upper face
h [mm]	0.5	11.4	0.1
θ	0	0	0
E_{11} [GPa]	70	3	70
E_{22} [GPa]	71	3	71
E_{33} [GPa]	69	2.8	69
G [GPa]	26	1	26
ν	0.3	0.25	0.3

A strong form solution can be obtained by means of a quasi-analytical Navier-type solution with a Fourier series expansion for representing the localized pressure load.

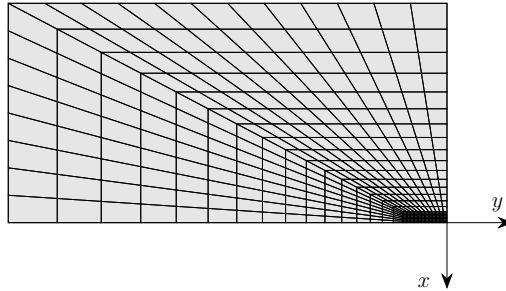


Figure 12: M-TC: Refined mesh in proximity of the localized pressure load.

The in-plane distributions for this benchmark are characterized by significant gradients in proximity of the localized pressure load. For this reason, a regular mesh is refined towards the plate center as illustrated in Fig. 12. Exploiting symmetry, only one-quarter of the plate needs to be modeled and it has been discretized with 8×12 elements.

Present FE results are compared in Tab. 5 against the results obtained with the Navier solution by considering the mixed model LM7. The values are evaluated at the top and bottom of the sandwich plate as well as at facesheet-core interfaces located at $z = 5.9$ and $z = -5.5$. The results provided by the FEM model are seen to closely match the reference ones, with an absolute percentage error less than 5%.

An assessment is next carried out to highlight the capability of SGUF models to accurately reproduce the sandwich plate response with a reduced number of DOFs when compared to the high-order full LW model LM7. The results of this analysis are summarized in Tab. 6. The variables u_z , σ_{xx} and σ_{zz} are evaluated at the center of the plate ($x = 0, y = 0$) and the transverse shear stress σ_{xz} at the boundary of the load application area, where its maximum

Table 5: M-TC: Comparison between Navier-type solution and FEM solution for the LM7 model

Model	z	u_z [mm]	σ_{xx} [MPa]	σ_{xz} [MPa]	σ_{zz} [MPa]
LM7 ^a	6	-3.78	-624	0	-1.04
	5.9 ⁺	-3.78	580	-0.17	-0.85
	-5.5 ⁻	-2.14	-138	-0.04	-0.18
	-6	-2.14	146	0	0
LM7	6	-3.73 (1.16%)	-625 (0.27%)	0 (0.00%)	-1 (4.00%)
	5.9 ⁺	-3.73 (1.16%)	582 (0.34%)	-0.17 (0.00%)	-0.83 (2.4%)
	-5.5 ⁻	-2.13 (0.47%)	-138 (0.00%)	-0.04 (0.00%)	-0.17 (5.55%)
	-6	-2.13 (0.47%)	146 (0.00%)	0 (0.00%)	0 (0.00%)

Table 6: M-TC: Assessment of classical and mixed SGUF models for the Meyer-Piening sandwich plate under a localized pressure load. The absolute percentage error is calculated w.r.t. LM7 solution.

Model (nDOF)	z	u_z [mm]	σ_{xx} [MPa]
LM7 (132)	6	-3.73 (-)	-625 (-)
	5.9 ⁺	-3.73 (-)	582 (-)
	-5.5 ⁻	-2.13 (-)	-138 (-)
	-6	-2.13 (-)	146 (-)
FSDT/FSDT (9)	6	-2.65 (28.95%)	-73 (88.32%)
	5.9 ⁺	-2.65 (28.95%)	39 (93.30%)
	-5.5 ⁻	-2.65 (24.41%)	-276 (100.00%)
	-6	-2.65 (24.41%)	283 (93.84%)
FSDT/ED ₃₂ (15)	6	-3.72 (0.27%)	-610 (2.4%)
	5.9 ⁺	-3.72 (0.27%)	567 (2.58%)
	-5.5 ⁻	-2.12 (0.47%)	-138 (0.00%)
	-6	-2.12 (0.47%)	146 (0.00%)
EM ₁₀ ² /EM ₃₂ ²¹ (31)	6	-3.73 (0.00%)	-613 (1.92%)
	5.9 ⁺	-3.73 (0.00%)	569 (2.23%)
	-5.5 ⁻	-2.13 (0.00%)	-139 (0.72%)
	-6	-2.13 (0.00%)	147 (0.68%)
EM ₁₀ ² /EM ₃₂ ²¹ (27)	6	-3.73 (0.00%)	-613 (1.92%)
	5.9 ⁺	-3.73 (0.00%)	580 (0.34%)
	-5.5 ⁻	-2.13 (0.00%)	-139 (0.72%)
	-6	-2.13 (0.00%)	147 (0.68%)

value is reached ($x = -2.5, y = 0$). Tab. 6 reports also the nodal DOF of the considered PVD-based and RMVT-based models.

Fig. 13 shows the transverse displacement u_z and the bending stress σ_{xx} distributions along two sections cut taken at $x = 0$ and $y = 0$, where $\bar{x} = 2x/a$ and $\bar{y} = 2y/b$ are the non-dimensional coordinates spanning the x and y directions respectively. The results show that the use of FSDT for modeling the core is not suitable for grasping the local indentation: the core kinematics must include the transverse normal stretch if the effect of the local pressure load is to be resolved. As long as the in-plane gradients of the response are concerned, no difference is appreciated between the mixed $EM_{10}^{2\cdot}/EM_{32}^{21}$ model and the displacement-based FSDT/ED₃₂ model.

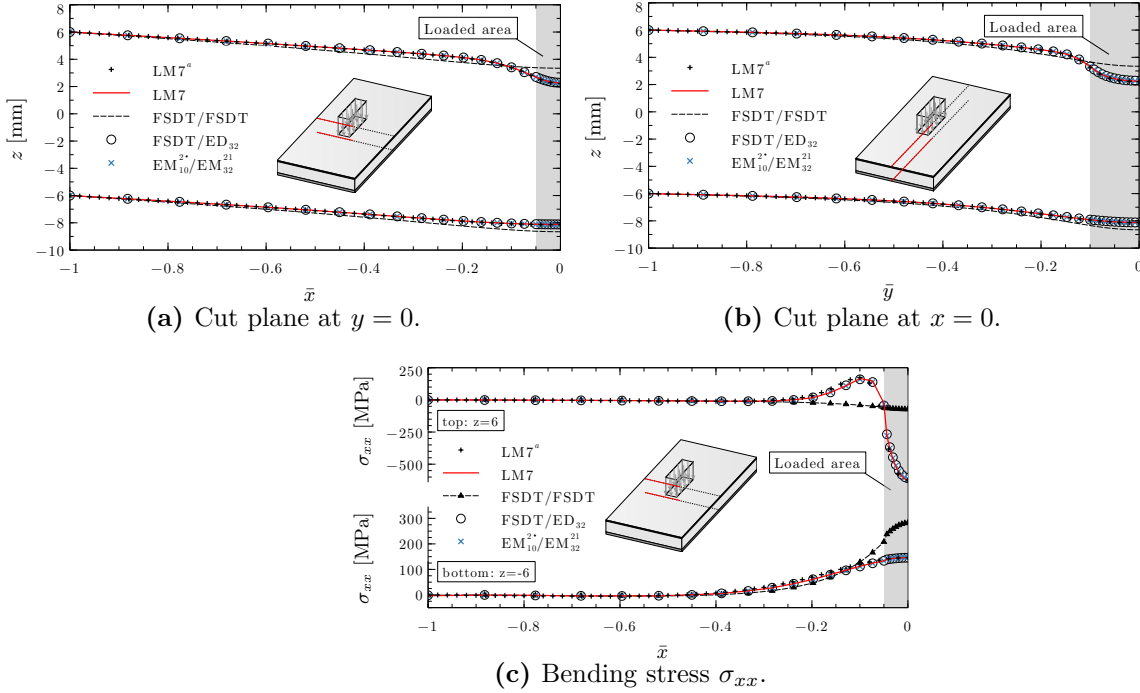


Figure 13: M-TC: In-plane distribution of coordinate z and bending stress σ_{xx} at top and bottom surfaces.

In order to appreciate the difference between the RMVT-based and PVD-based models, Fig. 14 reports the through-thickness distributions of the transverse displacement u_z , the bending stress σ_{xx} and the transverse stresses σ_{xz} and σ_{zz} . The improved transverse stress response of mixed models is obvious. Furthermore, it is possible to enhance the transverse stress approximation locally in the core and the facesheets so to very accurately retrieve the reference solution, see Fig. 14c and Fig. 14d. The effect is particularly emphasized of exactly satisfying the homogeneous stress conditions at the plate's top and bottom surfaces. It must be pointed out that the expansion orders for the transverse stress variables in RMVT models can not be freely chosen without considering the displacement field in order to avoid spurious oscillations [67]. For this reason, a richer kinematics for the displacement field must be used if the an enriched description of the transverse stress field is desired.

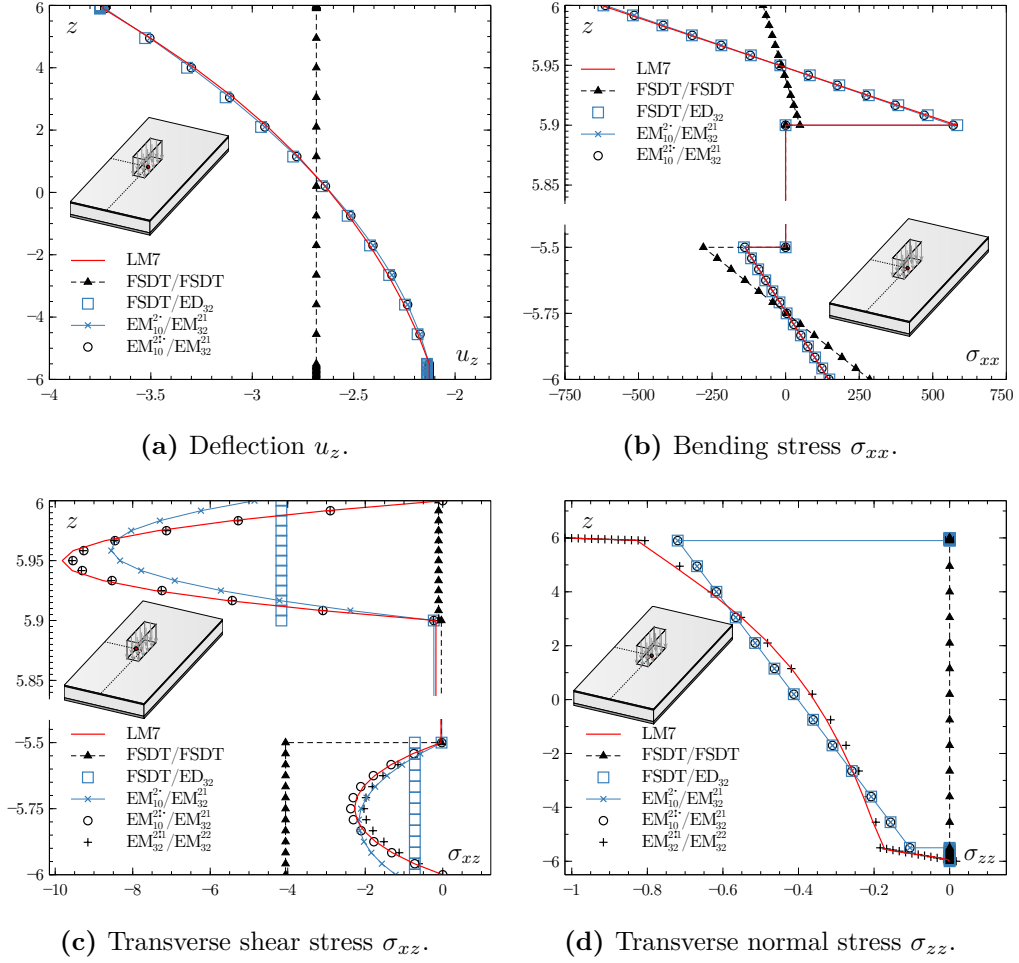


Figure 14: M-TC: Through-thickness distributions of deflection u_z , bending stress σ_{xx} and transverse stresses σ_{xz} and σ_{zz} .

4.4 Indentation benchmark

The indentation of a sandwich beam is finally investigated by referring to the problem considered by Navarro *et al.* [61] and, therefore, referred to as Navarro-TestCase (N-TC). The beam problem is defined in the (x, z) -plane as displayed in Fig. 15, with a concentrated load $P = 1000$ N acting at the centre of the beam at the top surface and the bottom of the beam fully clamped ($u_x = u_z = 0$). The data for geometry and material properties is given in Tab. 7. Symmetry is exploited to reduce the computational model to one-half of the beam.

Navarro *et al.* developed a very effective model for core crushing, which is based on a semi-analytical continuum-based model proposed by Vlasov [61]: considering a homogenous and isotropic core, its elastic response is given in terms of a simple two-parameters “elastic foundation” model, which relies upon the assumption of zero in-plane displacement in the core and on a decay function of the core deformation that annihilates the perturbation at the bottom of the core [68, 69].

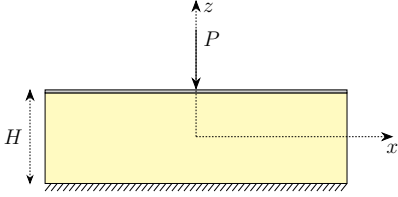


Figure 15: N-TC: Sandwich beam with indentation load.

Table 7: N-TC: Geometric and material data.

$a = 100 \text{ mm}; b = 1 \text{ mm}; H = 31 \text{ mm}$		
	Core	Upper face
h [mm]	30	1
θ	0	0
E_{11} [GPa]	0.2	100
E_{22} [GPa]	0.2	100
E_{33} [GPa]	0.2	100
G [GPa]	0.087	38.46
ν	0.15	0.3

In the following, present SGUF FEM results are compared against the semi-analytical Vlasov’s model as well as a reference elasticity solution obtained by the commercial FE package Abaqus. It will be shown that the present approach, which is more general than Vlasov’s “elastic foundation” model, is capable of providing very accurate results with only a 2D mesh and reduced number of DOF when compared to the commercial FE packages.

Following [61], the Abaqus model for one-half of the beam consists of 200 two-nodes shear-deformable plane beam elements (B21) for the facesheet and 4200 four-nodes plane stress elements (CPS4R) for the core. This results in a discrete model with 9805 DOF. The axial displacement u_x inside the core is suppressed in order to better reproduce Vlasov’s assumption.

The present SGUF models adopt FSDT for the facesheet and high-order models for the core, in which the axial displacement is expanded only linearly along the thickness in order to minimise the axial deformation of the core as per Vlasov’s assumption. High-order expansions are adopted for the transverse displacement in the core, ranging from cubic up to sixth-order: the core models are thus expressed as $ED_{1N_{u_z}}$ with $N_{u_z} \in \{3, \dots, 6\}$. As far as the 2D mesh is concerned, the beam is modeled with only one 4-node plate element across the width, by imposing $u_y = 0$. 50 elements are used along the beam axis, with a bias factor (the ratio of the largest edge size to the smallest) of 10 to increase the mesh density towards the loading area to accurately grasp the localized stress field.

The number of total DOF of the considered SGUF models is compared against the Abaqus model in Tab. 8.

Table 8: N-TC: DOFs comparison between commercial software FEM and 2D SGUF model.

Model	DOFs
ED ₁₃ /FSDT	1020
ED ₁₄ /FSDT	1122
ED ₁₅ /FSDT	1224
ED ₁₆ /FSDT	1326
Abaqus	9805

Fig. 16 shows the distributions along the beam axis (x -direction) of the transverse displacement u_z and bending stiffness σ_{xx} at the top of the skin ($z = H/2 = 15.5 \text{ mm}$), as well as the transverse shear stress σ_{xz} and the transverse normal stress σ_{zz} in the core just below the interface with the facesheet ($z = 14.5 \text{ mm}$). A very satisfying agreement of the SGUF model FSDT/ED₁₄ with the reference Abaqus solution is obtained. The discrepancy in the

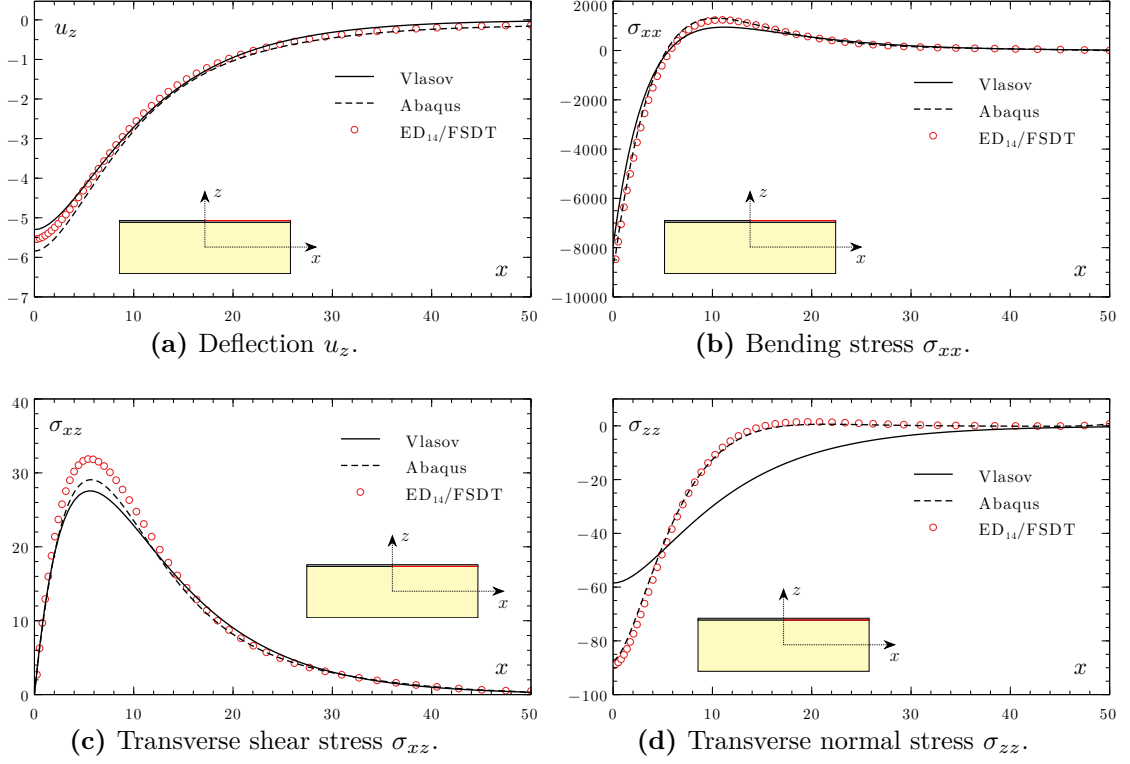


Figure 16: N-TC: In-plane distributions of deflection u_z , bending stress σ_{xx} in the skin and transverse stresses σ_{xz} and σ_{zz} in the foam.

maximum transverse shear stress (Fig. 16c) is attributed to the particular kinematics that has been adopted inside the core. Concerning Vlasov’s model, it is capable of very precisely reproducing the local indentation of the facesheet (transverse displacement and bending stress, see Fig. 16a and Fig. 16b), but the transverse stresses inside the core appear to be less accurate. In particular, the maximum value of the transverse normal stress predicted by Vlasov’s model in correspondence of the concentrated load is quite unsatisfactory (Fig. 16d).

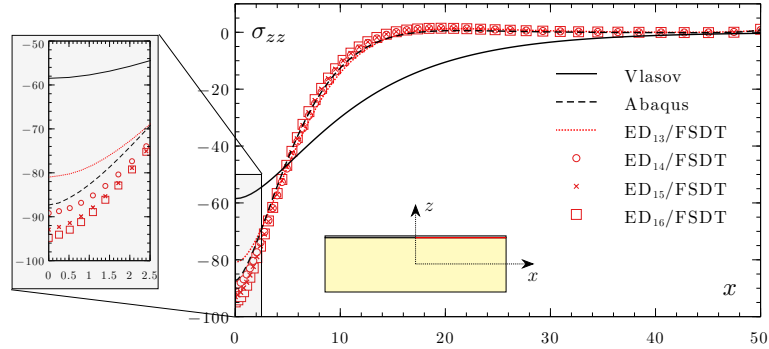


Figure 17: N-TC: Influence of out-of-plane displacement approximation order on transverse normal stress σ_{zz} .

Fig. 17 shows the convergence of transverse normal stress at the facesheet-core interface upon increasing the expansion order N_{u_z} , with emphasis on the region of the applied concentrated load. It can be seen that the maximum compressive stress appears to converge

towards a finite value of approximately -95 MPa. Therefore, the present SGUF modeling approach allows to recover full three-dimensional results with a simple 2D mesh and, hence, a reduced number of DOF compared to the standard FEM available in commercial packages (see Tab. 8).

5 Conclusion & Outlooks

This paper has extended for the first time the variable kinematics plate modeling approach referred to as Sublaminated Generalized Unified Formulation (SGUF), to the general Finite Element framework. Bi-linear four-nodes elements of general quadrilateral shape have been formulated for conventional displacement-based as well as RMVT-based mixed plate models. The adopted QC4 interpolation for the transverse shear strain makes the element locking-free and robust against distorted mesh. The proposed FE has been applied to investigate the static response of sandwich panels, ranging from global bending up to local indentation under a concentrated load. The results demonstrate the flexibility of the approach, that allows to adapt the number of DOF (i.e., the computational effort) depending on the desired accuracy and selecting independently the in-plane mesh density and the through-thickness model parameters. It has been shown that FE mesh refinement and dedicated high-order models for selected sublaminates allow to recover the complex three-dimensional response of the facesheets and the core with a number of DOF that is far below that required by currently available approaches in commercial FE packages.

Thanks to the promising results of the proposed SGUF-FEM approach, future developments shall be considered that extend its scope towards the dynamic analysis of viscoelastic sandwich plates as well as towards curved shell geometries. Future work will also address the inclusion of geometric non-linearities in view of stability analyses. Furthermore, it is worthwhile exploring the possibility to couple the variable kinematics approach offered by the SGUF with the FEM so to adopt different models in different elements within a global-local modeling strategy. Relevant literature to this topic is already available [70, 71]

A Matrices containing the thickness and in-plane interpolation functions

The arrays containing the through-thickness approximations and the shape functions (and their derivatives) introduced in the definition of the strain field in Eq. (18) are:

$$\mathbf{F}_{b\mu\mu}(z_p) = \begin{bmatrix} F_{\mu_{ux}}(z_p) & 0 & 0 & 0 \\ 0 & F_{\mu_{uy}}(z_p) & 0 & 0 \\ 0 & 0 & F_{\mu_{ux}}(z_p) & F_{\mu_{uy}}(z_p) \end{bmatrix} \quad (22)$$

$$\mathbf{F}_{n\mu\mu}(z_p) = [0 \ 0 \ F_{\mu_{uz,z}}(z_p)] \quad (23)$$

$$\mathbf{F}_{s\mu\mu}^0 = \begin{bmatrix} F_{\mu_{ux,z}}^0 & F_{\mu_{uy,z}}^0 & F_{\mu_{uz}}^0 & 0 & 0 & 0 \\ 0 & 0 & 0 & F_{\mu_{ux,z}}^0 & F_{\mu_{uy,z}}^0 & F_{\mu_{uz}}^0 \end{bmatrix} \quad (24)$$

$$\mathbf{F}_{s\mu\mu}^h(z_p) = \begin{bmatrix} F_{\mu_{ux,z}}^h(z_p) & 0 & F_{\mu_{uz}}^h(z_p) & 0 \\ 0 & F_{\mu_{uy,z}}^h(z_p) & 0 & F_{\mu_{uz}}^h(z_p) \end{bmatrix} \quad (25)$$

$$\mathbf{B}_{bi}(x, y) = \begin{bmatrix} N_{i,x}(x, y) & 0 & N_{i,y}(x, y) & 0 \\ 0 & N_{i,y}(x, y) & 0 & N_{i,x}(x, y) \\ 0 & 0 & 0 & 0 \end{bmatrix}^T \quad (26)$$

$$\mathbf{B}_{ni}(x, y) = \begin{bmatrix} 0 & 0 & 0 & 0 \\ 0 & 0 & 0 & 0 \\ 0 & 0 & 0 & N_i(x, y) \end{bmatrix}^T \quad (27)$$

$$\bar{\mathbf{B}}_{si}(x, y) = \begin{bmatrix} \mathcal{N}_i^{xu_x}(x, y) & 0 & 0 \\ 0 & \mathcal{N}_i^{xu_y}(x, y) & 0 \\ 0 & 0 & \mathcal{N}_i^{xu_z}(x, y) \\ \mathcal{N}_i^{yu_x}(x, y) & 0 & 0 \\ 0 & \mathcal{N}_i^{yu_y}(x, y) & 0 \\ 0 & 0 & \mathcal{N}_i^{yu_z}(x, y) \end{bmatrix} \quad (28)$$

$$\mathbf{B}_{si}(x, y) = \begin{bmatrix} N_i(x, y) & 0 & 0 & 0 \\ 0 & N_i(x, y) & 0 & 0 \\ 0 & 0 & N_{i,x}(x, y) & N_{i,y}(x, y) \end{bmatrix}^T \quad (29)$$

The isoparametric interpolation functions for the four-node element depicted in Fig. 2 are:

$$N_i(\xi, \eta) = \frac{1}{4} (1 + \xi_i \xi) (1 + \eta_i \eta) \quad (30)$$

where ξ_i and η_i are the natural coordinates of the i^{th} node.

B QC4 interpolation scheme

The modified field-compatible shape functions $\mathcal{N}_i^{r\mathcal{U}}$ (with $\mathcal{U} \in \{u_x, u_y, u_z\}$ and $r \in \{x, y\}$) used to interpolate the z -constant part of the transverse shear strains γ_{xz}^0 and γ_{yz}^0 in Eq. (28) are:

$$\begin{bmatrix} \mathcal{N}_i^x \\ \mathcal{N}_i^y \end{bmatrix}^{\mathcal{U}} = \mathbf{J}_{(GP)}^{-1} \begin{bmatrix} \mathcal{N}_i^\xi \\ \mathcal{N}_i^\eta \end{bmatrix}^{\mathcal{U}} = \begin{bmatrix} j_{11} & j_{12} \\ j_{21} & j_{22} \end{bmatrix}^{(GP)} \begin{bmatrix} \mathcal{N}_i^\xi \\ \mathcal{N}_i^\eta \end{bmatrix}^{\mathcal{U}} \quad (31)$$

where $j_{\alpha\beta}^{(GP)}$ (with $\alpha, \beta \in \{1, 2\}$) are the inverse terms of Jacobian matrix at Gauss point.

$$\begin{aligned}\mathcal{N}_i^{\xi\mathcal{U}} &= \sum_{I=1}^2 C_{\xi_I}(\xi, \eta) \gamma_i^{\xi\mathcal{U}}(\xi_I, \eta_I) \\ \mathcal{N}_i^{\eta\mathcal{U}} &= \sum_{J=1}^2 C_{\eta_J}(\xi, \eta) \gamma_i^{\eta\mathcal{U}}(\xi_J, \eta_J)\end{aligned}\quad (32)$$

where $\gamma_i^{\xi\mathcal{U}}$ and $\gamma_i^{\eta\mathcal{U}}$ are the transverse shear strains evaluated at tying points (Fig. 18) with

$$\begin{aligned}C_{\xi_1}(\xi, \eta) &= \frac{1-\eta}{2}; \quad C_{\xi_2}(\xi, \eta) = \frac{1+\eta}{2} \\ C_{\eta_1}(\xi, \eta) &= \frac{1-\xi}{2}; \quad C_{\eta_2}(\xi, \eta) = \frac{1+\xi}{2}\end{aligned}\quad (33)$$

Using Einstein notation, the transverse shear strains components in Eq. (32) are written as

$$\begin{aligned}\gamma_i^{\xi u_x}(\xi_I, \eta_I) &= N_i(\xi_I, \eta_I) J_{11}^{(I)}(\xi_I, \eta_I) + N_{i,\xi}^{RT}(\xi_I, \eta_I) \\ \gamma_i^{\xi u_y}(\xi_I, \eta_I) &= N_i(\xi_I, \eta_I) J_{12}^{(I)}(\xi_I, \eta_I) + N_{i,\xi}^{ST}(\xi_I, \eta_I) \\ \gamma_i^{\xi u_z}(\xi_I, \eta_I) &= N_{i,\xi}(\xi_I, \eta_I) \\ \gamma_i^{\eta u_x}(\xi_J, \eta_J) &= N_i(\xi_J, \eta_J) J_{21}^{(J)}(\xi_J, \eta_J) + N_{i,\eta}^{RT}(\xi_J, \eta_J) \\ \gamma_i^{\eta u_y}(\xi_J, \eta_J) &= N_i(\xi_J, \eta_J) J_{22}^{(J)}(\xi_J, \eta_J) + N_{i,\eta}^{ST}(\xi_J, \eta_J) \\ \gamma_i^{\eta u_z}(\xi_J, \eta_J) &= N_{i,\eta}(\xi_J, \eta_J)\end{aligned}\quad (34)$$

where $J_{\alpha\beta}^{(t)}$ (with $t \in \{1, 2\}$) are the terms of Jacobian matrix evaluated at tying point t . The functions N_i^{RT} and N_i^{ST} for the four-node element are given as:

$$\begin{aligned}N_{i|i=1,2}^{RT}(\xi, \eta) &= \frac{1}{8} \left[(-1)^i J_{11}^{(i)} \xi (1 - \xi^2) (1 + \eta_i \eta) - J_{21}^{(i)} (1 + \xi_i \xi) \eta (1 - \eta^2) \right] \\ N_{i|i=3,4}^{RT}(\xi, \eta) &= \frac{1}{8} \left[(-1)^{i+1} J_{11}^{(i)} \xi (1 - \xi^2) (1 + \eta_i \eta) + J_{21}^{(i)} (1 + \xi_i \xi) \eta (1 - \eta^2) \right] \\ N_{i|i=1,2}^{ST}(\xi, \eta) &= \frac{1}{8} \left[(-1)^i J_{12}^{(i)} \xi (1 - \xi^2) (1 + \eta_i \eta) - J_{22}^{(i)} (1 + \xi_i \xi) \eta (1 - \eta^2) \right] \\ N_{i|i=3,4}^{ST}(\xi, \eta) &= \frac{1}{8} \left[(-1)^{i+1} J_{12}^{(i)} \xi (1 - \xi^2) (1 + \eta_i \eta) + J_{22}^{(i)} (1 + \xi_i \xi) \eta (1 - \eta^2) \right]\end{aligned}\quad (35)$$

where $J_{\alpha\beta}^{(i)}$ are the terms of Jacobian matrix at node i .

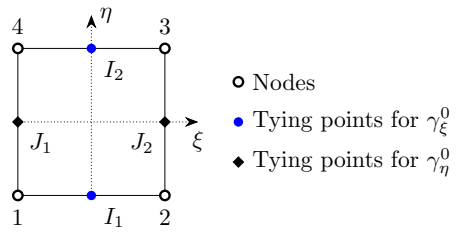


Figure 18: Tying points for the QC4 interpolation functions.

C Kernels of the Sublaminar-Generalized Unified Formulation

C.1 Displacement-based formulation

The fundamental nuclei of the displacement-based formulation derived from Eq. (6) are

$$\begin{aligned}
K_{u_x u_x}^{p\mu_{u_x} \tau_{u_x} ij} &= Z_{u_x u_x 11}^{p\mu_{u_x} \tau_{u_x}} \langle N_{i,x} N_{j,x} \rangle_{\Omega} + Z_{u_x u_x 16}^{p\mu_{u_x} \tau_{u_x}} \langle N_{i,y} N_{j,x} \rangle_{\Omega} + \\
&+ Z_{u_x u_x 16}^{p\mu_{u_x} \tau_{u_x}} \langle N_{i,x} N_{j,y} \rangle_{\Omega} + Z_{u_x u_x 66}^{p\mu_{u_x} \tau_{u_x}} \langle N_{i,y} N_{j,y} \rangle_{\Omega} + \\
&+ Z_{u_x u_x 44}^{p\mu_{u_x, z} \tau_{u_x, z} 00} \langle \mathcal{N}_i^{y u_x} \mathcal{N}_j^{y u_x} \rangle_{\Omega} + Z_{u_x u_x 45}^{p\mu_{u_x, z} \tau_{u_x, z} 00} \langle \mathcal{N}_i^{x u_x} \mathcal{N}_j^{y u_x} \rangle_{\Omega} + \\
&+ Z_{u_x u_x 45}^{p\mu_{u_x, z} \tau_{u_x, z} 00} \langle \mathcal{N}_i^{y u_x} \mathcal{N}_j^{x u_x} \rangle_{\Omega} + Z_{u_x u_x 45}^{p\mu_{u_x, z} \tau_{u_x, z} h0} \langle N_i \mathcal{N}_j^{y u_x} \rangle_{\Omega} + \\
&+ Z_{u_x u_x 45}^{p\mu_{u_x, z} \tau_{u_x, z} 0h} \langle \mathcal{N}_i^{y u_x} N_j \rangle_{\Omega} + Z_{u_x u_x 55}^{p\mu_{u_x, z} \tau_{u_x, z} 00} \langle \mathcal{N}_i^{x u_x} \mathcal{N}_j^{x u_x} \rangle_{\Omega} + \\
&+ Z_{u_x u_x 55}^{p\mu_{u_x, z} \tau_{u_x, z} 0h} \langle \mathcal{N}_i^{x u_x} N_j \rangle_{\Omega} + Z_{u_x u_x 55}^{p\mu_{u_x, z} \tau_{u_x, z} h0} \langle N_i \mathcal{N}_j^{x u_x} \rangle_{\Omega} + \\
&+ Z_{u_x u_x 55}^{p\mu_{u_x, z} \tau_{u_x, z} hh} \langle N_i N_j \rangle_{\Omega} \\
K_{u_x u_y}^{p\mu_{u_x} \tau_{u_y} ij} &= Z_{u_x u_y 12}^{p\mu_{u_x} \tau_{u_y}} \langle N_{i,x} N_{j,y} \rangle_{\Omega} + Z_{u_x u_y 26}^{p\mu_{u_x} \tau_{u_y}} \langle N_{i,y} N_{j,y} \rangle_{\Omega} + \\
&+ Z_{u_x u_y 16}^{p\mu_{u_x} \tau_{u_y}} \langle N_{i,x} N_{j,x} \rangle_{\Omega} + Z_{u_x u_y 66}^{p\mu_{u_x} \tau_{u_y}} \langle N_{i,y} N_{j,x} \rangle_{\Omega} + \\
&+ Z_{u_x u_y 44}^{p\mu_{u_x, z} \tau_{u_y, z} 00} \langle \mathcal{N}_i^{y u_x} \mathcal{N}_j^{y u_y} \rangle_{\Omega} + Z_{u_x u_y 44}^{p\mu_{u_x, z} \tau_{u_y, z} 0h} \langle \mathcal{N}_i^{y u_x} N_j \rangle_{\Omega} + \\
&+ Z_{u_x u_y 45}^{p\mu_{u_x, z} \tau_{u_y, z} 00} \langle \mathcal{N}_i^{x u_x} \mathcal{N}_j^{y u_y} \rangle_{\Omega} + Z_{u_x u_y 45}^{p\mu_{u_x, z} \tau_{u_y, z} 00} \langle \mathcal{N}_i^{y u_x} \mathcal{N}_j^{x u_y} \rangle_{\Omega} + \\
&+ Z_{u_x u_y 45}^{p\mu_{u_x, z} \tau_{u_y, z} 0h} \langle \mathcal{N}_i^{x u_x} N_j \rangle_{\Omega} + Z_{u_x u_y 45}^{p\mu_{u_x, z} \tau_{u_y, z} h0} \langle N_i \mathcal{N}_j^{y u_y} \rangle_{\Omega} + \\
&+ Z_{u_x u_y 45}^{p\mu_{u_x, z} \tau_{u_y, z} hh} \langle N_i N_j \rangle_{\Omega} + Z_{u_x u_y 55}^{p\mu_{u_x, z} \tau_{u_y, z} 00} \langle \mathcal{N}_i^{x u_x} \mathcal{N}_j^{x u_y} \rangle_{\Omega} + \\
&+ Z_{u_x u_y 55}^{p\mu_{u_x, z} \tau_{u_y, z} h0} \langle N_i \mathcal{N}_j^{x u_y} \rangle_{\Omega} \\
K_{u_x u_z}^{p\mu_{u_x} \tau_{u_z} ij} &= Z_{u_x u_z 13}^{p\mu_{u_x} \tau_{u_z}} \langle N_{i,x} N_j \rangle_{\Omega} + Z_{u_x u_z 36}^{p\mu_{u_x} \tau_{u_z}} \langle N_{i,y} N_j \rangle_{\Omega} + \\
&+ Z_{u_x u_z 44}^{p\mu_{u_x, z} \tau_{u_z} 00} \langle \mathcal{N}_i^{y u_x} \mathcal{N}_j^{y u_z} \rangle_{\Omega} + Z_{u_x u_z 44}^{p\mu_{u_x, z} \tau_{u_z} 0h} \langle \mathcal{N}_i^{y u_x} N_{j,y} \rangle_{\Omega} + \\
&+ Z_{u_x u_z 45}^{p\mu_{u_x, z} \tau_{u_z} 00} \langle \mathcal{N}_i^{x u_x} \mathcal{N}_j^{y u_z} \rangle_{\Omega} + Z_{u_x u_z 45}^{p\mu_{u_x, z} \tau_{u_z} 00} \langle \mathcal{N}_i^{y u_x} \mathcal{N}_j^{x u_z} \rangle_{\Omega} + \\
&+ Z_{u_x u_z 45}^{p\mu_{u_x, z} \tau_{u_z} 0h} \langle \mathcal{N}_i^{y u_x} N_{j,x} \rangle_{\Omega} + Z_{u_x u_z 45}^{p\mu_{u_x, z} \tau_{u_z} h0} \langle \mathcal{N}_i^{x u_x} N_{j,y} \rangle_{\Omega} +
\end{aligned} \tag{36}$$

$$\begin{aligned}
& + Z_{u_x u_z 45}^{p\mu_{u_x, z} \tau_{u_z} h0} \triangleleft N_i \mathcal{N}_j^{y u_z} \triangleright_{\Omega} + Z_{u_x u_z 45}^{p\mu_{u_x, z} \tau_{u_z} h h} \triangleleft N_i N_{j, y} \triangleright_{\Omega} + \\
& + Z_{u_x u_z 55}^{p\mu_{u_x, z} \tau_{u_z} 00} \triangleleft \mathcal{N}_i^{x u_x} \mathcal{N}_j^{x u_z} \triangleright_{\Omega} + Z_{u_x u_z 55}^{p\mu_{u_x, z} \tau_{u_z} 0 h} \triangleleft \mathcal{N}_i^{x u_x} N_{j, x} \triangleright_{\Omega} + \\
& + Z_{u_x u_z 55}^{p\mu_{u_x, z} \tau_{u_z} h0} \triangleleft N_i \mathcal{N}_j^{x u_z} \triangleright_{\Omega} + Z_{u_x u_z 55}^{p\mu_{u_x, z} \tau_{u_z} h h} \triangleleft N_i N_{j, x} \triangleright_{\Omega}
\end{aligned}$$

$$\begin{aligned}
K_{u_y u_y}^{p\mu_{u_y} \tau_{u_y} i j} & = Z_{u_y u_y 22}^{p\mu_{u_y} \tau_{u_y}} \triangleleft N_{i, y} N_{j, y} \triangleright_{\Omega} + Z_{u_y u_y 26}^{p\mu_{u_y} \tau_{u_y}} \triangleleft N_{i, x} N_{j, y} \triangleright_{\Omega} + \\
& + Z_{u_y u_y 26}^{p\mu_{u_y} \tau_{u_y}} \triangleleft N_{i, y} N_{j, x} \triangleright_{\Omega} + Z_{u_y u_y 66}^{p\mu_{u_y} \tau_{u_y}} \triangleleft N_{i, x} N_{j, x} \triangleright_{\Omega} + \\
& + Z_{u_y u_y 44}^{p\mu_{u_y, z} \tau_{u_y, z} 00} \triangleleft \mathcal{N}_i^{y u_y} \mathcal{N}_j^{y u_y} \triangleright_{\Omega} + Z_{u_y u_y 44}^{p\mu_{u_y, z} \tau_{u_y, z} h0} \triangleleft N_i \mathcal{N}_j^{y u_y} \triangleright_{\Omega} + \\
& + Z_{u_y u_y 44}^{p\mu_{u_y, z} \tau_{u_y, z} 0 h} \triangleleft \mathcal{N}_i^{y u_y} N_j \triangleright_{\Omega} + Z_{u_y u_y 44}^{p\mu_{u_y, z} \tau_{u_y, z} h h} \triangleleft N_i N_j \triangleright_{\Omega} + \\
& + Z_{u_y u_y 45}^{p\mu_{u_y, z} \tau_{u_y, z} 00} \triangleleft \mathcal{N}_i^{x u_y} \mathcal{N}_j^{y u_y} \triangleright_{\Omega} + Z_{u_y u_y 45}^{p\mu_{u_y, z} \tau_{u_y, z} 00} \triangleleft \mathcal{N}_i^{y u_y} \mathcal{N}_j^{x u_y} \triangleright_{\Omega} + \\
& + Z_{u_y u_y 45}^{p\mu_{u_y, z} \tau_{u_y, z} 0 h} \triangleleft \mathcal{N}_i^{x u_y} N_j \triangleright_{\Omega} + Z_{u_y u_y 45}^{p\mu_{u_y, z} \tau_{u_y, z} h0} \triangleleft N_i \mathcal{N}_j^{x u_y} \triangleright_{\Omega} + \\
& + Z_{u_y u_y 55}^{p\mu_{u_y, z} \tau_{u_y, z} 00} \triangleleft \mathcal{N}_i^{x u_y} \mathcal{N}_j^{x u_y} \triangleright_{\Omega}
\end{aligned}$$

$$\begin{aligned}
K_{u_y u_z}^{p\mu_{u_y} \tau_{u_z} i j} & = Z_{u_y u_z 23}^{p\mu_{u_y} \tau_{u_z}} \triangleleft N_{i, y} N_j \triangleright_{\Omega} + Z_{u_y u_z 36}^{p\mu_{u_y} \tau_{u_z}} \triangleleft N_{i, x} N_j \triangleright_{\Omega} + \\
& + Z_{u_y u_z 44}^{p\mu_{u_y, z} \tau_{u_z} 00} \triangleleft \mathcal{N}_i^{y u_y} \mathcal{N}_j^{y u_z} \triangleright_{\Omega} + Z_{u_y u_z 44}^{p\mu_{u_y, z} \tau_{u_z} 0 h} \triangleleft \mathcal{N}_i^{y u_y} N_{j, y} \triangleright_{\Omega} + \\
& + Z_{u_y u_z 44}^{p\mu_{u_y, z} \tau_{u_z} h0} \triangleleft N_i \mathcal{N}_j^{y u_z} \triangleright_{\Omega} + Z_{u_y u_z 44}^{p\mu_{u_y, z} \tau_{u_z} h h} \triangleleft N_i N_{j, y} \triangleright_{\Omega} + \\
& + Z_{u_y u_z 45}^{p\mu_{u_y, z} \tau_{u_z} 00} \triangleleft \mathcal{N}_i^{x u_y} \mathcal{N}_j^{y u_z} \triangleright_{\Omega} + Z_{u_y u_z 45}^{p\mu_{u_y, z} \tau_{u_z} 00} \triangleleft \mathcal{N}_i^{y u_y} \mathcal{N}_j^{x u_z} \triangleright_{\Omega} + \\
& + Z_{u_y u_z 45}^{p\mu_{u_y, z} \tau_{u_z} 0 h} \triangleleft \mathcal{N}_i^{y u_y} N_{j, x} \triangleright_{\Omega} + Z_{u_y u_z 45}^{p\mu_{u_y, z} \tau_{u_z} 0 h} \triangleleft \mathcal{N}_i^{x u_y} N_{j, y} \triangleright_{\Omega} + \\
& + Z_{u_y u_z 45}^{p\mu_{u_y, z} \tau_{u_z} h0} \triangleleft N_i \mathcal{N}_j^{x u_z} \triangleright_{\Omega} + Z_{u_y u_z 45}^{p\mu_{u_y, z} \tau_{u_z} h h} \triangleleft N_i N_{j, x} \triangleright_{\Omega} + \\
& + Z_{u_y u_z 55}^{p\mu_{u_y, z} \tau_{u_z} 00} \triangleleft \mathcal{N}_i^{x u_y} \mathcal{N}_j^{x u_z} \triangleright_{\Omega} + Z_{u_y u_z 55}^{p\mu_{u_y, z} \tau_{u_z} 0 h} \triangleleft \mathcal{N}_i^{x u_y} N_{j, x} \triangleright_{\Omega} +
\end{aligned}$$

$$\begin{aligned}
K_{u_z u_z}^{p\mu_{u_z} \tau_{u_z} i j} & = Z_{u_z u_z 33}^{p\mu_{u_z} \tau_{u_z}} \triangleleft N_i N_j \triangleright_{\Omega} + Z_{u_z u_z 44}^{p\mu_{u_z} \tau_{u_z} 00} \triangleleft \mathcal{N}_i^{y u_z} \mathcal{N}_j^{y u_z} \triangleright_{\Omega} + \\
& + Z_{u_z u_z 44}^{p\mu_{u_z} \tau_{u_z} 0 h} \triangleleft \mathcal{N}_i^{y u_z} N_{j, y} \triangleright_{\Omega} + Z_{u_z u_z 44}^{p\mu_{u_z} \tau_{u_z} h0} \triangleleft N_{i, y} \mathcal{N}_j^{y u_z} \triangleright_{\Omega} +
\end{aligned}$$

$$\begin{aligned}
& + Z_{u_z u_z 44}^{p\mu_{u_z} \tau_{u_z} hh} \triangleleft N_{i,y} N_{j,y} \triangleright \Omega + Z_{u_z u_z 45}^{p\mu_{u_z} \tau_{u_z} 00} \triangleleft \mathcal{N}_i^{xu_z} \mathcal{N}_j^{yu_z} \triangleright \Omega + \\
& + Z_{u_z u_z 45}^{p\mu_{u_z} \tau_{u_z} 00} \triangleleft \mathcal{N}_i^{yu_z} \mathcal{N}_j^{xu_z} \triangleright \Omega + Z_{u_z u_z 45}^{p\mu_{u_z} \tau_{u_z} 0h} \triangleleft \mathcal{N}_i^{yu_z} N_{j,x} \triangleright \Omega + \\
& + Z_{u_z u_z 45}^{p\mu_{u_z} \tau_{u_z} 0h} \triangleleft \mathcal{N}_i^{xu_z} N_{j,y} \triangleright \Omega + Z_{u_z u_z 45}^{p\mu_{u_z} \tau_{u_z} h0} \triangleleft N_{i,y} \mathcal{N}_j^{xu_z} \triangleright \Omega + \\
& + Z_{u_z u_z 45}^{p\mu_{u_z} \tau_{u_z} h0} \triangleleft N_{i,x} \mathcal{N}_j^{yu_z} \triangleright \Omega + Z_{u_z u_z 45}^{p\mu_{u_z} \tau_{u_z} hh} \triangleleft N_{i,y} N_{j,x} \triangleright \Omega + \\
& + Z_{u_z u_z 45}^{p\mu_{u_z} \tau_{u_z} hh} \triangleleft N_{i,x} N_{j,y} \triangleright \Omega + Z_{u_z u_z 55}^{p\mu_{u_z} \tau_{u_z} 00} \triangleleft \mathcal{N}_i^{xu_z} \mathcal{N}_j^{xu_z} \triangleright \Omega + \\
& + Z_{u_z u_z 55}^{p\mu_{u_z} \tau_{u_z} 0h} \triangleleft \mathcal{N}_i^{xu_z} N_{j,x} \triangleright \Omega + Z_{u_z u_z 55}^{p\mu_{u_z} \tau_{u_z} h0} \triangleleft N_{i,x} \mathcal{N}_j^{xu_z} \triangleright \Omega + \\
& + Z_{u_z u_z 55}^{p\mu_{u_z} \tau_{u_z} hh} \triangleleft N_{i,x} N_{j,x} \triangleright \Omega
\end{aligned}$$

where $\triangleleft \triangleright \Omega$ denotes the integration over the in-plane domain Ω .

C.2 RMVT-based formulation

The fundamental nuclei of the RMVT-based formulation derived from Eq. (7) are

$$\begin{aligned}
K_{u_x u_x}^{p\mu_{u_x} \tau_{u_x} ij} &= Z_{u_x u_x 11}^{p\mu_{u_x} \tau_{u_x}} \triangleleft N_{i,x} N_{j,x} \triangleright \Omega + Z_{u_x u_x 16}^{p\mu_{u_x} \tau_{u_x}} \triangleleft N_{i,y} N_{j,x} \triangleright \Omega + \\
& + Z_{u_x u_x 16}^{p\mu_{u_x} \tau_{u_x}} \triangleleft N_{i,x} N_{j,y} \triangleright \Omega + Z_{66 u_x u_x}^{p\mu_{u_x} \tau_{u_x}} \triangleleft N_{i,y} N_{j,y} \triangleright \Omega \\
K_{u_x u_y}^{p\mu_{u_x} \tau_{u_y} ij} &= Z_{u_x u_y 12}^{p\mu_{u_x} \tau_{u_y}} \triangleleft N_{i,x} N_{j,y} \triangleright \Omega + Z_{u_x u_y 26}^{p\mu_{u_x} \tau_{u_y}} \triangleleft N_{i,y} N_{j,y} \triangleright \Omega + \\
& + Z_{u_x u_y 16}^{p\mu_{u_x} \tau_{u_y}} \triangleleft N_{i,x} N_{j,x} \triangleright \Omega + Z_{u_x u_y 66}^{p\mu_{u_x} \tau_{u_y}} \triangleleft N_{i,y} N_{j,x} \triangleright \Omega \\
K_{u_x s_x}^{p\mu_{u_x} \tau_{s_x} ij} &= Z_{u_x s_x}^{p\mu_{u_x, z} \tau_{s_x} 0a} \triangleleft \mathcal{N}_i^{xu_x} N_j \triangleright \Omega + Z_{u_x s_x}^{p\mu_{u_x, z} \tau_{s_x} ha} \triangleleft N_i N_j \triangleright \Omega \\
K_{u_x s_y}^{p\mu_{u_x} \tau_{s_y} ij} &= Z_{u_x s_y}^{p\mu_{u_x, z} \tau_{s_y} 0a} \triangleleft \mathcal{N}_i^{yu_x} N_j \triangleright \Omega \\
K_{u_x s_z}^{p\mu_{u_x} \tau_{s_z} ij} &= Z_{u_x s_z 13}^{p\mu_{u_x} \tau_{s_z}} \triangleleft N_{i,x} N_j \triangleright \Omega + Z_{u_x s_z 63}^{p\mu_{u_x} \tau_{s_z}} \triangleleft N_{i,y} N_j \triangleright \Omega \\
K_{u_y u_y}^{p\mu_{u_y} \tau_{u_y} ij} &= Z_{u_y u_y 22}^{p\mu_{u_y} \tau_{u_y}} \triangleleft N_{i,y} N_{j,y} \triangleright \Omega + Z_{u_y u_y 26}^{p\mu_{u_y} \tau_{u_y}} \triangleleft N_{i,x} N_{j,y} \triangleright \Omega + \\
& + Z_{u_y u_y 26}^{p\mu_{u_y} \tau_{u_y}} \triangleleft N_{i,y} N_{j,x} \triangleright \Omega + Z_{u_y u_y 66}^{p\mu_{u_y} \tau_{u_y}} \triangleleft N_{i,x} N_{j,x} \triangleright \Omega \\
K_{u_y s_x}^{p\mu_{u_y} \tau_{s_x} ij} &= Z_{u_y s_x}^{p\mu_{u_y, z} \tau_{s_x} 0a} \triangleleft \mathcal{N}_i^{xu_y} N_j \triangleright \Omega \\
K_{u_y s_y}^{p\mu_{u_y} \tau_{s_y} ij} &= Z_{u_y s_y}^{p\mu_{u_y, z} \tau_{s_y} 0a} \triangleleft \mathcal{N}_i^{yu_y} N_j \triangleright \Omega + Z_{u_y s_y}^{p\mu_{u_y, z} \tau_{s_y} ha} \triangleleft N_i N_j \triangleright \Omega \\
K_{u_y s_z}^{p\mu_{u_y} \tau_{s_z} ij} &= Z_{u_y s_z 23}^{p\mu_{u_y} \tau_{s_z}} \triangleleft N_{i,y} N_j \triangleright \Omega + Z_{u_y s_z 63}^{p\mu_{u_y} \tau_{s_z}} \triangleleft N_{i,x} N_j \triangleright \Omega
\end{aligned} \tag{37}$$

$$\begin{aligned}
K_{u_z s_x}^{p\mu_{u_z} \tau_{s_x} ij} &= Z_{u_z s_x}^{p\mu_{u_z} \tau_{s_x} 0a} \langle N_i^{xuz} N_j \rangle_\Omega + Z_{u_z s_x}^{p\mu_{u_z} \tau_{s_x} ha} \langle N_{i,x} N_j \rangle_\Omega \\
K_{u_z s_y}^{p\mu_{u_z} \tau_{s_y} ij} &= Z_{u_z s_y}^{p\mu_{u_z} \tau_{s_y} 0a} \langle N_i^{yuz} N_j \rangle_\Omega + Z_{u_z s_y}^{p\mu_{u_z} \tau_{s_y} ha} \langle N_{i,y} N_j \rangle_\Omega \\
K_{u_z s_z}^{p\mu_{u_z} \tau_{s_z} ij} &= Z_{u_z s_z}^{p\mu_{u_z, z} \tau_{s_z}} \langle N_i N_j \rangle_\Omega \\
K_{s_x s_x}^{p\mu_{s_x} \tau_{s_x} ij} &= -Z_{s_x s_x 55}^{p\mu_{s_x} \tau_{s_x}} \langle N_i N_j \rangle_\Omega \\
K_{s_x s_y}^{p\mu_{s_x} \tau_{s_y} ij} &= -Z_{s_x s_y 45}^{p\mu_{s_x} \tau_{s_y}} \langle N_i N_j \rangle_\Omega \\
K_{s_y s_y}^{p\mu_{s_y} \tau_{s_y} ij} &= -Z_{s_y s_y 44}^{p\mu_{s_y} \tau_{s_y}} \langle N_i N_j \rangle_\Omega \\
K_{s_z s_z}^{p\mu_{s_z} \tau_{s_z} ij} &= -Z_{s_z s_z 33}^{p\mu_{s_z} \tau_{s_z}} \langle N_i N_j \rangle_\Omega
\end{aligned} \tag{38}$$

References

- [1] B. Castanié, C. Bouvet, M. Ginot, Review of composite sandwich structure in aeronautic applications, *Compos. C* 1 (2020) 100004. doi:10.1016/j.jcomc.2020.100004
- [2] G. Palomba, G. Epasto, V. Crupi, Lightweight sandwich structures for marine applications: a review, *Mech. Adv. Mater. Struct.* (2021) 1–26. doi:10.1080/15376494.2021.1941448
- [3] J. M. Davies (Ed.), *Lightweight Sandwich Construction*, Blackwell Science Ltd., 2001.
- [4] J. R. Vinson, *The Behavior of Sandwich Structures of Isotropic and Composite Materials*, Technomic Publishing Co., 1999.
- [5] P. Resende Oliveira, M. May, T. Hallak Panzera, S. Hiermaier, Bio-based/green sandwich structures: A review, *Thin-Wall. Struct.* 177 (2022) 109426. doi:10.1016/j.tws.2022.109426
- [6] E. Carrera, S. Brischetto, A survey with numerical assessment of classical and refined theories for the analysis of sandwich plates, *Appl. Mech. Rev.* 62 (2009) 1–17. doi:10.1115/1.3013824
- [7] I. M. Daniel, E. E. Gdoutos, K.-A. Wang, J. L. Abot, Failure modes of composite sandwich beams, *Int. J. Damage Mech.* 11 (2002) 309–334. doi:10.1106/105678902027247
- [8] L. A. Carlsson, G. A. Kardomateas, *Structural and Failure Mechanics of Sandwich Composites*, Springer, 2011.
- [9] V. Birman, G. A. Kardomateas, Review of current trends in research and applications of sandwich structures, *Compos. B* 142 (2018) 221–240. doi:10.1016/j.compositesb.2018.01.027
- [10] A. D. Hasanyan, A. M. Waas, Micropolar constitutive relations for cellular solids, *J. Appl. Mech.* 83 (2016) 041001–1:10. doi:10.1115/1.4032115

- [11] A. T. Karttunen, J. N. Reddy, J. Romanoff, Two-scale micropolar plate model for web-core sandwich panels, *Int. J. Solids Struct.* 170 (2019) 82–94. doi:10.1016/j.ijsolstr.2019.04.026
- [12] F. Tornabene, M. Viscoti, R. Dimitri, M. A. Aiello, Higher order formulations for doubly-curved shell structures with a honeycomb core, *Thin-Wall. Struct.* 164 (2021) 107789. doi:10.1016/j.tws.2021.107789
- [13] W. S. Burton, A. K. Noor, Assessment of computational models for sandwich panels and shells, *Comput. Meth. Appl. Mech. Eng.* 124 (1995) 125–151. doi:10.1016/0045-[]7825(94)00750-[]H
- [14] A. K. Noor, W. S. Burton, Computational models for sandwich panels and shells, *Appl. Mech. Rev.* 49 (1996) 155–199. doi:10.1115/1.3101923
- [15] H. Hu, S. Belouettar, M. Potier-Ferry, E. M. Daya, Review and assessment of various theories for modeling sandwich composites, *Compos. Struct.* 84 (2008) 282–292. doi:10.1016/j.compstruct.2007.08.007
- [16] I. Kreja, A literature review on computational models for laminated composite and sandwich panels, *Cent. Eur. J. Engng.* 1 (2011) 59–80. doi:10.2478/s13531-[]011-[]0005-[]x
- [17] A. S. Sayyad, Y. M. Ghugal, On the free vibration analysis of laminated composite and sandwich plates: A review of recent literature with some numerical results, *Compos. Struct.* 129 (2015) 177–201. doi:10.1016/j.compstruct.2015.04.007
- [18] M. F. Caliri, A. J. M. Ferreira, V. Tita, A review on plate and shell theories for laminated and sandwich structures highlighting the finite element method, *Compos. Struct.* 156 (2016) 63–77, 70th Anniversary of Professor J. N. Reddy. doi:10.1016/j.compstruct.2016.02.036
- [19] S. Irfan, F. Siddiqui, A review of recent advancements in finite element formulation for sandwich plates, *Chinese J. Aero.* 34 (2019) 785–798. doi:10.1016/j.cja.2018.11.011
- [20] F. Siddiqui, G. A. Kardomateas, Extended higher-order sandwich panel theory for plates with arbitrary aspect ratios, *J. Mech. Mater. Struct.* 14 (4) (2019) 449–459. doi:10.2140/jomms.2019.14.449
- [21] F. Siddiqui, G. A. Kardomateas, Nonlinear static analysis of plates with arbitrary aspect ratios using Extended Higher Order Sandwich Panel Theory, *Int. J. Non-Lin. Mech.* 132 (2021) 103701. doi:10.1016/j.ijnonlinmec.2021.103701
- [22] V. L. Berdichevsky, Variational-asymptotic method of constructing a theory of shells, *J. Appl. Math. Mech. (P. M. M.)* 43 (1979) 711–736. doi:10.1016/0021-[]8928(79)90157-[]6
- [23] V. L. Berdichevsky, An asymptotic theory of sandwich plates, *Int. J. Eng. Sci.* 48 (2010) 383–404. doi:10.1016/j.ijengsci.2009.09.001

- [24] S. Lee, C.-Y. Lee, D. H. Hodges, On the mechanics of composite sandwich plates with three-dimensional stress recovery, *Int. J. Eng. Sci.* 157 (2020) 103406. doi:10.1016/j.ijengsci.2020.103406
- [25] E. Carrera, Theories and finite elements for multilayered plates and shells: A unified compact formulation with numerical assessment and benchmarking, *Arch. Comput. Meth. Eng.* 10 (2003) 215–296. doi:10.1007/BF02736224
- [26] E. Carrera, M. Cinefra, M. Petrolo, E. Zappino, *Finite Element Analysis of Structures through Unified Formulation*, John Wiley & Sons, Ltd, 2014.
- [27] L. Demasi, ∞^3 Hierarchy plate theories for thick and thin composite plates: The generalized unified formulation, *Compos. Struct.* 84 (2008) 256–270. doi:10.1016/j.compstruct.2007.08.004
- [28] L. Demasi, ∞^6 Mixed plate theories based on the generalized unified formulation. Part I: Governing equations, *Compos. Struct.* 87 (2009) 1–11. doi:10.1016/j.compstruct.2008.07.013
- [29] L. Demasi, Partially Layer Wise advanced Zig Zag and HSDT models based on the Generalized Unified Formulation, *Eng. Struct.* 53 (2013) 63–91. doi:10.1016/j.engstruct.2013.01.021
- [30] E. Reissner, On a certain mixed variational theorem and a proposed application, *Int. J. Numer. Meth. Eng.* 20 (1984) 1366–1368. doi:10.1002/nme.1620200714
- [31] E. Reissner, On a mixed variational theorem and on a shear deformable plate theory, *Int. J. Numer. Meth. Eng.* 23 (1986) 193–198. doi:10.1002/nme.1620230203
- [32] E. Carrera, C_z^0 -Requirements - models for the two dimensional analysis of multilayered structures, *Compos. Struct.* 37 (1997) 373–383. doi:10.1016/S0263-[]8223(98)80005-[]6
- [33] E. Carrera, Historical review of Zig-Zag theories for multilayered plates and shells, *Appl. Mech. Rev.* 56 (1983) 287–308. doi:10.1115/1.1557614
- [34] H. Murakami, Laminated composite plate theory with improved in-plane responses, *J. Appl. Mech.* 53 (1986) 661–666. doi:10.1115/1.3171828.
- [35] A. Tessler, M. Di Sciuva, M. Gherlone, A consistent refinement of first-order shear deformation theory for laminated composite and sandwich plates using improved zigzag kinematics, *J. Mech. Mater. Struct.* 5 (2010) 341–347. doi:10.2140/jomms.2010.5.341.
- [36] L. Iurlaro, M. Gherlone, M. Di Sciuva, A. Tessler, Refined Zigzag Theory for laminated composite and sandwich plates derived from Reissner’s Mixed Variational Theorem, *Compos. Struct.* 133 (2015) 809–817. doi:10.1016/j.compstruct.2015.08.004.
- [37] M. Gherlone, On the Use of Zigzag Functions in Equivalent Single Layer Theories for Laminated Composite and Sandwich Beams: A Comparative Study and Some Observations on External Weak Layers, *J. Appl. Mech.* 80 (2013) 061004-1-19. doi:10.1115/1.4023690.

- [38] R. M. J. Groh, P. M. Weaver On displacement-based and mixed-variational equivalent single layer theories for modelling highly heterogeneous laminated beams, *Int. J. Solids Struct.* 59 (2015) 147–170. doi:10.1016/j.ijsolstr.2015.01.020.
- [39] L. Demasi, 2D, Quasi 3D and 3D exact solutions for bending of thick and thin sandwich plates, *J. Sandwich Struct. Mater.* 10 (2008) 271–310. doi:10.1177/1099636208089311
- [40] L. Demasi, W. Yu, Assess the accuracy of the variational asymptotic plate and shell analysis using the generalized unified formulation, *Mech. Adv. Mater. Struct.* 20 (2013) 227–241. doi:10.1080/15376494.2011.584150
- [41] D. S. Mashat, E. Carrera, A. M. Zenkour, S. A. Al Khateeb, Axiomatic/asymptotic evaluation of multilayered plate theories by using single and multi-points error criteria, *Compos. Struct.* 106 (2013) 393–406. doi:10.1016/j.compstruct.2013.05.047
- [42] M. Petrolo, A. Lamberti, Axiomatic/asymptotic analysis of refined layer-wise theories for composite and sandwich plates, *Mech. Adv. Mater. Struct.* 23 (2015) 28–42. doi:10.1080/15376494.2014.924607
- [43] M. Petrolo, M. Cinefra, A. Lamberti, E. Carrera, Evaluation of mixed theories for laminated plates through the axiomatic/asymptotic method, *Compos. B* 76 (2015) 260–272. doi:10.1016/j.compositesb.2015.02.027
- [44] M. D’Ottavio, A Sublaminated Generalized Unified Formulation for the analysis of composite structures and its application to sandwich plates bending, *Compos. Struct.* 142 (2016) 187–199. doi:10.1016/j.compstruct.2016.01.087.
- [45] M. Botshekanan Dehkordi, M. Cinefra, S. M. R. Khalili, E. Carrera, Mixed LW/ESL models for the analysis of sandwich plates with composite faces, *Compos. Struct.* 98 (2013) 330–339. doi:10.1016/j.compstruct.2012.11.016
- [46] M. D’Ottavio, L. Dozio, R. Vescovini, O. Polit, Bending analysis of composite laminated and sandwich structures using sublaminated variable-kinematic Ritz models, *Compos. Struct.* 155 (2016) 45–62. doi:10.1016/j.compstruct.2016.07.036.
- [47] R. Vescovini, M. D’Ottavio, L. Dozio, O. Polit, Buckling and wrinkling of anisotropic sandwich plates, *Int. J. Eng. Sci.* 130 (2018) 136–156. doi:10.1016/j.ijengsci.2018.05.010.
- [48] A. Gorgeri, R. Vescovini, L. Dozio, Analysis of multiple-core sandwich cylindrical shells using a sublaminated formulation, *Compos. Struct.* 225 (2019) 111067. doi:10.1016/j.compstruct.2019.111067
- [49] M. D’Ottavio, A. Krasnobrizha, E. Valot, O. Polit, R. Vescovini, L. Dozio, Dynamic response of viscoelastic multiple-core sandwich structures, *J. Sound Vib.* 491 (2021) 115753. doi:10.1016/j.jsv.2020.115753.
- [50] E. Carrera, M. Cinefra, P. Nali, MITC technique extended to variable kinematic multilayered plate elements, *Compos. Struct.* 92 (2010) 1888–1895. doi:10.1016/j.compstruct.2010.01.009.

- [51] M. Cinefra, M. D'Ottavio, O. Polit, E. Carrera, Assessment of MITC plate elements based on CUF with respect to distorted meshes, *Compos. Struct.* 238 (2020) 111962. doi:10.1016/j.compstruct.2020.111962.
- [52] G. M. Kulikov, S. V. Plotnikova, A hybrid-mixed four-node quadrilateral plate element based on sampling surfaces method for 3D stress analysis, *Int. J. Numer. Meth. Engng.* 108 (2016) 26–54. doi:10.1002/nme.5201.
- [53] G. M. Kulikov, S. V. Plotnikova, Hybrid-mixed ANS finite elements for stress analysis of laminated composite structures: Sampling surfaces plate formulation, *Comput. Methods Appl. Mech. Eng.* 303 (2016) 374–399. doi:10.1016/j.cma.2016.01.015.
- [54] G. M. Kulikov, S. V. Plotnikova, E. Carrera, A robust, four-node, quadrilateral element for stress analysis of functionally graded plates through higher-order theories, *Mech. Adv. Mater. Struct.* 25 (2018) 1383–1402. doi:10.1080/15376494.2017.1288994.
- [55] T. H. C. Le, M. D'Ottavio, P. Vidal, O. Polit, A new robust quadrilateral four-node variable kinematics plate element for composite structures, *Finite Elem. Anal. Des.* 133 (2017) 10–24. doi:10.1016/j.finel.2017.05.002.
- [56] T. H. C. Le, M. D'Ottavio, P. Vidal, O. Polit, Robust displacement and mixed CUF-based four-node and eight-node quadrilateral plate elements, in: H. Altenbach, E. Carrera, G. Kulikov (Eds.), *Analysis and Modelling of Advanced Structures and Smart Systems*, Vol. 81 of *Advanced Structured Materials*, Springer, Singapore, 2018, Ch. 6, pp. 89–118. doi:10.1007/978-[]981-[]10-[]6895-[]9_6.
- [57] J. Reddy, *Mechanics of Laminated Composite Plates and Shells: Theory and Analysis*, Second Edition, Taylor & Francis, 2004.
- [58] G. A. Kardomateas, C. N. Phan, Three-dimensional elasticity solution for sandwich beams/wide plates with orthotropic phases: The negative discriminant case, *J. Sandwich Struct. Mater.* 13 (6) (2011) 641–661. doi:10.1177/1099636211419127
- [59] H.-R. Meyer-Piening, Application of the elasticity solution to linear sandwich beam, plate and shell analyses, *J. Sandwich Struct. Mater.* 6 (2004) 295–312. doi:10.1177/1099636204035395.
- [60] Z. Yuan, G. A. Kardomateas, Y. Frostig, Geometric nonlinearity effects in the response of sandwich wide panels, *J. Appl. Mech.* 83 (2016). doi:10.1115/1.4033651.
- [61] P. Navarro, S. Abrate, J. Aubry, S. Marguet, J.-F. Ferrero, Analytical modeling of indentation of composite sandwich beam, *Compos. Struct.* 100 (2013) 79–88. doi:10.1016/j.compstruct.2012.12.017.
- [62] C. N. Phan, Y. Frostig, G. A. Kardomateas, Analysis of sandwich beams with a compliant core and with in-plane rigidity—extended high-order sandwich panel theory versus elasticity, *J. Appl. Mech.* 79 (2012) 041001–1:11. doi:10.1115/1.4005550.

- [63] V. S. Sokolinsky, H. Shen, L. Vaikhanski, S. R. Nutt, Experimental and analytical study of nonlinear bending response of sandwich beams, *Compos. Struct.* 60 (2003) 219–229. doi:10.1016/s0263-[]8223(02)00293-[]3.
- [64] R. M. J. Groh, P. M. Weaver Static inconsistencies in certain axiomatic higher-order shear deformation theories for beams, plates and shells, *Compos. Struct.* 120 (2015) 231–245. doi:10.1016/j.compstruct.2014.10.006.
- [65] N. J. Pagano, Exact solutions for rectangular bidirectional composites and sandwich plates, *J. Compos. Mater.* 4 (1970) 20–34. doi:10.1177/002199837000400102.
- [66] G. A. Kardomateas, Three-dimensional elasticity solution for sandwich plates with orthotropic phases: The positive discriminant case, *J. Appl. Mech.* 76 (2009) 0145505–1:4. doi:10.1115/1.2966174
- [67] L. Demasi, ∞^6 mixed plate theories based on the generalized unified formulation. part v: Results, *Compos. Struct.* 88 (1) (2009) 1–16. doi:10.1016/j.compstruct.2008.07.009.
- [68] U. N. Leontev, V. Z. Vlasov, *Beams, plates and shells on elastic foundations*, Israel Program for Scientific Translations (translated from Russian), Jerusalem, 1966.
- [69] I.-B. Teodoru, EBBEF2p – A computer code for analyzing beams on elastic foundations, *Intersections* 6 (2009) 28–44.
- [70] C. Wenzel, P. Vidal, M. D’Ottavio, O. Polit, Coupling of heterogeneous kinematics and finite element approximations applied to composite beam structures, *Compos. Struct.* 116 (2014) 177–192. doi:10.1016/j.compstruct.2014.04.022.
- [71] E. Zappino, G. Li, A. Pagani, E. Carrera, Global-local analysis of laminated plates by node-dependent kinematic finite elements with variable ESL/LW capabilities, *Compos. Struct.* 172 (2017) 1–14. doi:10.1016/j.compstruct.2017.03.057